Research Square

Preprints are preliminary reports that have not undergone peer review.
They should not be considered conclusive, used to inform clinical practice,
or referenced by the media as validated information.

Mechanistic Investigation of a Novel Astragalus Polysaccharide Compound in the Treatment of Iron-Deficiency Anemia Based on Gut Microbiota Modulation

yili han
Shanxi University of Traditional Chinese Medicine
yu zhang
Shanxi University of Traditional Chinese Medicine
yanhui wu
Shanxi University of Traditional Chinese Medicine
ziying lei
Shanxi University of Traditional Chinese Medicine
shengting zhao
Shanxi University of Traditional Chinese Medicine
huifang li
Shanxi University of Traditional Chinese Medicine
runli he
herunli@sxtcm.edu.cn

Shanxi University of Traditional Chinese Medicine

Research Article

Keywords: Astragalus polysaccharides, polysaccharide-iron(II) complexes, anti-iron-deficiency anemia, gut microbiota

Posted Date: August 10th, 2026

DOI: https://doi.org/10.21203/rs.3.rs-10203004/v1

License: This work is licensed under a Creative Commons Attribution 4.0 International License.
Read Full License

Additional Declarations: No competing interests reported.

Mechanistic Investigation of a Novel *Astragalus* Polysaccharide Compound in the Treatment of Iron-Deficiency Anemia Based on Gut Microbiota Modulation

Yi-li Han[1]，Yu Zhnag[1]，Yan-hui Wu[1]，Zi-ying Lei[1]，Shengting Zhao[1]，Hui-fang Li[1]，Run-li He

Abstract

To develop a novel polysaccharide-ferrous iron supplement with high efficacy and low toxicity, *Astragalus* polysaccharides (APS) and Fe^{2+} were employed as primary substrates to synthesize an *Astragalus* polysaccharide-iron(II) complex (APS-iron(II)). The contents of neutral sugars, proteins, and Fe^{2+} were quantitatively determined using the phenol-sulfuric acid method, Coomassie Brilliant Blue assay, and o-phenanthroline method, respectively. An iron-deficiency anemia (IDA) rat model was established to evaluate therapeutic efficacy. Hematological parameters, serum iron metabolism indices, and antioxidant enzyme activities were assessed across multiple groups, including the normal control, model, ferrous succinate (FS), Polysaccharide Iron Complex Capsules (PIC), APS, APS-iron(III), and low-, medium-, and high-dose APS-iron(II) groups. Histopathological alterations in the liver, spleen, and kidney were examined, and 16S rRNA sequencing was conducted to characterize gut microbiota composition, thereby elucidating the anti-anemic effects and underlying mechanisms.The APS-iron(II) complex contains 75.32 ± 4.28% neutral sugars and 0.94 ± 0.74% protein, with an iron content of 7.83 ± 0.64%. Its monosaccharide composition consists of glucose (Glc), galactose (Gal), and arabinose (Ara) in a molar ratio of 85.26:10.69:4.05. APS-iron(II) significantly improved erythrocyte parameters in IDA rats, exhibiting superior iron supplementation and hematopoietic effects compared with the APS-iron(III) group. Notably, the medium- and high-dose APS-iron(II) groups outperformed the positive control treatments. In addition, APS-iron(II) markedly alleviated histopathological damage in hepatic, splenic, and renal tissues and enhanced hepatic iron storage.Gut microbiota analysis revealed that IDA markedly reduced microbial richness and diversity, characterized by a decrease in the relative abundance of Firmicutes and an increase in Bacteroidetes. Treatment with APS-iron(II) restored microbial diversity, increased the abundance of beneficial genera such as *Lactobacillus* and *Bifidobacterium*, and decreased the abundance of potentially pathogenic genera, including *Desulfovibrio* and *Clostridium sensu stricto 1*. Correlation analysis further indicated that *Lactobacillus* and *Bifidobacterium* were positively associated with erythrocyte parameters, whereas genera such as *Romboutsia* exhibited significant negative correlations. Collectively, these findings suggest that APS-iron(II) exerts pronounced anti-iron-deficiency anemia effects by improving iron metabolism, enhancing antioxidant capacity, and modulating the composition and abundance of the gut microbiota. Its efficacy surpasses that of commonly used clinical iron supplements, thereby providing robust experimental evidence and a theoretical foundation for the development of novel polysaccharide-based iron formulations.

Keywords *Astragalus* polysaccharides·polysaccharide-iron(II) complexes·anti-iron-deficiency anemia·gut microbiota

Abbreviations

APS *Astragalus membranaceus* Polysaccharide
IDA Iron deficiency anemia
APS-iron (II) *Astragalus membranaceus* Polysaccharide-Iron (II)
APS-iron (III) *Astragalus membranaceus* Polysaccharide-Iron (III)
FS ferrous succinate
PIC polysaccharide-iron complex capsules

Introduction

According to statistics from the World Health Organization (WHO), approximately 2 billion people worldwide suffer from anemia, accounting for nearly 30% of the global population, and roughly 50% of these cases are attributed to iron-deficiency anemia (IDA)[1]. IDA impairs oxygen transport capacity, disrupts energy metabolism, and inhibits cellular growth and proliferation[2]. Moreover, it has been associated with immune dysfunction, neurocognitive impairment, and alterations in gut microbial composition[3,4]. Consequently, iron supplementation remains the primary strategy for the prevention and treatment of IDA and for the restoration of body iron stores[5].

Currently, the most commonly prescribed iron supplements in clinical practice are ferrous salts, including ferrous sulfate, ferrous succinate, and ferrous fumarate[6,7]. However, accumulating evidence indicates that prolonged administration of free Fe^{2+} may cause gastrointestinal irritation, nausea, vomiting, and other adverse effects, thereby limiting patient compliance[8,9]. Therefore, the development of effective, safe, and low-toxicity iron supplements has become an important research objective.

In recent years, increasing attention has been directed toward novel ferric iron formulations, such as polysaccharide-iron complexes, ferric succinate, and polypeptide-iron chelates[10]. In polysaccharide-iron(III) complexes, coordination between Fe^{3+} and the polysaccharide matrix not only preserves the biological activity of the macromolecule but also enables the polysaccharide component to exert synergistic anti-anemic effects while reducing gastrointestinal irritation[11-14]. Among potential polysaccharide candidates, *Astragalus membranaceus* is particularly attractive. The dried roots of *Astragalus membranaceus* (Fisch.) Bge. or *Astragalus membranaceus* var. *mongholicus* (Bge.) are widely recognized as medicinal and edible homologous materials in traditional Chinese medicine. As a principal component of the classical prescription Danggui Buxue Decoction, *Astragalus* has long been used for replenishing qi and nourishing the blood[15,16].

Astragalus polysaccharides (APS), one of the major bioactive constituents of *Astragalus*, possess abundant hydroxyl, carboxyl, and other functional groups, making them excellent ligands for metal ion coordination. These structural features may facilitate the absorption and utilization of Fe^{2+} within the gastrointestinal tract. In contrast, Fe^{3+} in polysaccharide-iron(III) complexes is prone to hydrolysis under intestinal pH conditions, resulting in the formation of insoluble polyoxo-hydroxide precipitates. Consequently, ferric iron generally exhibits lower bioavailability than ferrous iron and often requires a longer supplementation period to achieve therapeutic efficacy[17,18].

In addition to disturbances in iron metabolism, emerging evidence has demonstrated that IDA profoundly alters the balance, diversity, and composition of the gut microbiota, leading to microbial dysbiosis. Given the pivotal role of gut microorganisms in nutrient absorption, immune regulation, and host metabolism, modulation of the gut microbiota has become a promising

therapeutic approach for improving IDA outcomes.

Based on the complementary advantages of polysaccharide-based carriers and ferrous iron supplementation, the present study exploited the medicinal and nutritional properties of Astragalus and its traditional functions of replenishing qi, promoting hematopoiesis, and nourishing the blood. APS was employed as a natural coordinating ligand and complexed with Fe^{2+} to synthesize an *Astragalus* polysaccharide-iron(II) complex (APS-iron(II)). The therapeutic efficacy of this novel complex against iron-deficiency anemia was subsequently evaluated, with particular emphasis on its regulatory effects on the gut microbiota. The findings of this study provide a theoretical basis for elucidating the anti-anemic mechanisms of polysaccharide-ferrous complexes mediated through gut microbiota modulation and may contribute to the development of next-generation iron supplements with enhanced efficacy and safety profiles.

Materials and Methods

Preparation of *Astragalus* Polysaccharides

The Astragali Radix decoction pieces (batch no. 230402) obtained from Shanxi Yuanhetang Traditional Chinese Medicine Co., Ltd. were pulverized and subsequently passed through a 40-mesh sieve. An accurately weighed portion of 50.00 g of the resulting powder was transferred into a 1000 mL round-bottom flask, followed by the addition of 150 mL of 75% ethanol for desorption over 40 min. Subsequently, distilled water was added at a solid-liquid ratio of 1:12, and the mixture was subjected to reduced-pressure distillation at 80 °C for 6 min[19]. The extract was then filtered under vacuum, and the residue was re-extracted twice under identical conditions.The combined filtrates were concentrated to 250 mL, after which absolute ethanol was added to achieve a final ethanol concentration of 80% (v/v). The solution was allowed to stand overnight and then vacuum-filtered. Proteins were removed using the Sevag method, followed by decolorization with macroporous resin. The solution was subsequently filtered, concentrated, and lyophilized. The obtained product was accurately weighed to yield *Astragalus* polysaccharides.

Preparation of APS-iron(II) complex

Preparation of Ferrous Solution:Ferric chloride hexahydrate ($FeCl_3 \cdot 6H_2O$, 50.0 mg, obtained from Tianjin Kermel Chemical Reagent Co., Ltd.)was accurately weighed and transferred into a 100 mL volumetric flask, followed by dilution to volume with distilled water to yield a ferric chloride solution with a concentration of 0.1 mg/mL. An aliquot of 5.0 mL of this solution was precisely transferred into a 25 mL volumetric flask. Subsequently, 6 mL of 4% ascorbic acid solution (purchased from Shanghai Macklin Biochemical Technology Co., Ltd.) was added, followed by the sequential addition of 1.0 mL of 36% dilute acetic acid, 1.5 mL of 1 mol/L sodium acetate, and 1.0 mL of 0.15% o-phenanthroline solution (supplied by Tianjin Kaitong Chemical Reagent Co., Ltd.). The mixture was diluted to volume, thoroughly mixed, and allowed to stand for 10 min, at which point the Fe^{2+} concentration was determined to be 2.378 μg/mL.

Chemical composition analysis

Determination of Neutral Sugar Content

Preparation of Reference Solution:Anhydrous glucose reference standard (14.1 mg), obtained from Shanghai Ronghe Pharmaceutical Technology Co., Ltd., was accurately weighed, dissolved in distilled water, and quantitatively transferred into a 100 mL volumetric flask. The solution was diluted to volume and thoroughly mixed to obtain a standard solution with a final concentration of 0.141 mg/mL.

Construction of the Standard Curve:Aliquots of 0.00, 0.25, 0.30, 0.35, 0.45, 0.60, 0.70, and 0.90 mL of the reference solution were precisely transferred into 10 mL colorimetric tubes, and distilled water was

added to adjust the volume to 1.0 mL. Subsequently, 0.6 mL of 5% phenol solution was added, followed by the slow and continuous addition of 3.0 mL of concentrated sulfuric acid. The mixtures were allowed to stand for 2 min, thoroughly mixed, and then subjected to color development in a boiling water bath for 20 min. After cooling to room temperature, the absorbance (*A*) was measured at 490 nm using the corresponding reagent blank as the reference. A standard calibration curve was constructed by plotting concentration against absorbance.

Preparation of Sample Solutions:*Astragalus* polysaccharide (APS, 5.0 mg), the total APS-iron(II) complex derived from 5.0 mg APS, and the APS-iron(III) complex were accurately weighed and individually dissolved in distilled water, followed by dilution to 10 mL in volumetric flasks to obtain the respective sample solutions.

Determination:An aliquot of 1.0 mL of each sample solution was precisely transferred into a 10 mL colorimetric tube and analyzed according to the procedure described above. The absorbance (*A*) was measured, and the neutral sugar contents of APS, APS-iron(II), APS-iron (III), and APS-iron(III) complexes were calculated based on the corresponding standard calibration curve.

Determination of protein content

The protein content variations in Astragalus polysaccharide (APS), APS-iron(II), and APS-iron(III) complexes were quantitatively determined using the Coomassie Brilliant Blue assay[20].

Determination of Fe^{2+} Content

Preparation of Standard Solution and Calibration Curve:Ferrous sulfate heptahydrate ($FeSO_4 \cdot 7H_2O$, 49.65 mg), obtained from Tianjin Kaitong Chemical Reagent Co., Ltd., was accurately weighed, dissolved in distilled water, and diluted to volume in a 100 mL volumetric flask. An aliquot of 5.0 mL of this solution was then precisely transferred into a 25 mL volumetric flask and diluted to volume, yielding a Fe^{2+} standard solution with a concentration of 19.86 μg/mL.Aliquots of 0.0, 1.0, 2.0, 3.0, 4.0, and 5.0 mL of the standard solution were accurately transferred into separate 25 mL volumetric flasks. Subsequently, 1.0 mL of 0.15% o-phenanthroline solution and 1.5 mL of 1 mol/L sodium acetate solution were added sequentially, and the mixtures were diluted to volume with distilled water. After standing for 10 min, the absorbance (*A*) of each standard solution was measured at 511 nm using the corresponding reagent blank as the reference. A calibration curve was constructed by plotting Fe^{2+} concentration against absorbance[21].

Determination of Sample Fe^{2+} Content: Aliquots (1.0 mL) of APS sample solution, as well as the APS-iron(II) and APS-iron(III) complex solutions derived from 5.0 mg APS, were accurately transferred into separate 25 mL volumetric flasks. Subsequently, 0.6 mL of dilute acetic acid, 1.0 mL of 0.15% o-phenanthroline solution, and 1.5 mL of 1 mol/L sodium acetate solution were added in sequence, followed by dilution to volume with distilled water. The reaction mixtures were incubated in a water bath at 50 °C for 15 min and then cooled to room temperature. The absorbance was measured at 511 nm, and the Fe^{2+} content was calculated based on the corresponding calibration curve.

Changes in monosaccharide composition

Chromatographic Conditions:Chromatographic separation was performed using a Dionex CarboPac PA20 column (150 × 3.0 mm, 10 μm). The injection volume was 5 μL. The mobile phase consisted of solvent A (H_2O), solvent B (0.1 M NaOH), and solvent C (0.1 M NaOH containing 0.2 M NaAc). The flow rate was maintained at 0.5 mL/min, and the column temperature was set at 30 °C.The gradient elution program was as follows: 0 min, A/B/C = 95:5:0 (v/v); 26 min, 85:5:10 (v/v); 42 min, 85:5:10 (v/v); 42.1 min, 60:0:40 (v/v); 52 min, 60:40:0 (v/v); 52.1 min, 95:5:0 (v/v); and 60 min, 95:5:0 (v/v).

Preparation of Reference Solutions:Individual reference standards were accurately weighed and dissolved in water to prepare stock solutions at a concentration of 10 mg/mL. Appropriate aliquots of each stock solution were then combined to obtain mixed standard solutions with maximum concentrations of 60 μg/mL, 50 μg/mL, or 40 μg/mL, depending on the analyte.

Construction of Calibration Curves:Aliquots of the aforementioned mixed reference solutions were precisely transferred and analyzed under the chromatographic conditions described above according to the gradient scheme presented in Table 1. The corresponding peak areas were determined, and calibration curves were established by plotting peak area (y-axis) against mass concentration (x-axis), followed by linear regression analysis.

Tab 1 Information on Gradient Concentrations of Monosaccharide Mixtures

Name	*C*（μg/mL）					
Fuc	0.4	0.8	4	8	16	24
Rha	0.4	0.8	4	8	16	24
Ara	0.4	0.8	4	8	16	24
Gal	0.4	0.8	4	8	16	24
Glc	0.4	0.8	4	8	16	24
Xyl	0.4	0.8	4	8	16	24
Man	0.5	1	5	10	20	30
Fru	0.6	1.2	6	12	24	36
Rib	0.6	1.2	6	12	24	36
Gal-UA	0.6	1.2	6	12	24	36
Gul-UA	0.6	1.2	6	12	24	36
Glc-UA	0.6	1.2	6	12	24	36
Man-UA	0.6	1.2	6	12	24	36

Animal experiment design

Seventy-two female Wistar rats were housed under controlled environmental conditions (temperature: 22 ± 2 ℃; relative humidity: 55 ± 5%) with a simulated natural light-dark cycle (12 h light/12 h dark) to ensure physiological stability. After a one-week acclimatization period, blood samples were collected via the tail vein for the determination of hematological parameters, including hemoglobin (HGB), red blood cell count (RBC), hematocrit (HCT), mean corpuscular volume (MCV), mean corpuscular hemoglobin (MCH), and mean corpuscular hemoglobin concentration (MCHC).

The animals were randomly divided into two groups: a normal control group (n = 8) and an experimental group (n = 64). The control group was fed a standard diet, whereas the experimental group received a low-iron diet combined with repeated tail vein blood sampling (three times per week, for a total of 12 samplings). All animals had free access to purified water, and stainless steel cages were used to minimize exogenous iron contamination.

After 4 weeks, hematological indices (HGB, RBC, HCT, MCV, MCH, and MCHC) were re-evaluated in the experimental group. A hemoglobin level below 100 g/L was considered indicative of successful establishment of the iron-deficiency anemia (IDA) model[22].

The 64 IDA rats were then randomly assigned to the following groups: model group (IDA), ferrous succinate group (FS), positive control group receiving polysaccharide-iron complex

capsules (PIC), low-, medium-, and high-dose APS-iron(II) groups (L-, M-, and H-APS-iron(II)), APS group, and APS-iron(III) group. The control and IDA groups were administered sterile normal saline via oral gavage once daily. The FS group, PIC group, APS-iron(II) low-, medium-, and high-dose groups, and APS-iron(III) group were orally administered iron at doses of 27, 13.5, 6.8, 13.5, 27, and 13.5 mg/kg, respectively, once daily. The APS group received APS aqueous solution at a dose of 150 mg/kg per day via oral gavage. The treatment period lasted for 4 weeks. Body weight was recorded weekly.

Following overnight fasting, the rats were anesthetized with urethane, and blood samples were collected from the abdominal aorta. Hematological parameters were analyzed using an automated hematology analyzer. Additionally, the organ indices of the heart, liver, spleen, and kidneys were determined.

Determination of Serum Iron Parameters and Antioxidant Enzyme Activities:

Whole blood samples were collected into anticoagulant-free tubes and allowed to stand, followed by immediate centrifugation (4000 r/min, 4 °C, 10 min) to obtain serum for subsequent analyses. Commercial biochemical and enzyme-linked immunosorbent assay (ELISA) kits provided by Jiangsu Meimian Industrial Co., Ltd. were employed to determine serum iron (SI), total iron-binding capacity (TIBC), transferrin saturation (TS), erythropoietin (EPO) levels, as well as the activities of superoxide dismutase (SOD), malondialdehyde (MDA), catalase (CAT), and glutathione peroxidase (GSH-Px).

Determination of Hepatic Antioxidant Enzyme Activities (ELISA):

Liver tissues were collected and stored at -80 °C. Frozen liver samples were homogenized in physiological saline at a mass-to-volume ratio of 1:9 (g/mL) to obtain 10% (w/v) tissue homogenates. The homogenates were centrifuged at 4000 r/min for 15 min at 4 °C, and the supernatants were collected. The activities of SOD, MDA, CAT, and GSH-Px in liver tissues were determined according to the manufacturer's instructions using the corresponding ELISA kits.

Histopathological Analysis:

Fresh liver, spleen, and kidney tissues were fixed in 4% paraformaldehyde, followed by hematoxylin and eosin (H&E) staining. Histopathological evaluation was performed using an inverted microscope (Olympus Corporation, Tokyo, Japan). Additionally, Prussian blue staining was conducted on liver sections to assess iron deposition and distribution.

High-Throughput Sequencing Analysis of Gut Microbiota:

Microbial genomic DNA was extracted from fecal samples using a commercial stool DNA extraction kit. Amplification and sequencing of the V3-V4 regions of the 16S rRNA gene were performed by Jiangsu Sanshu Biotechnology Co., Ltd. (Nantong, China). All sequencing data were analyzed using the online Sanshu Cloud Platform.

Statistical Analysis

All experimental data are expressed as mean ± standard deviation ($\bar{x} \pm s$). Statistical analyses were conducted using SPSS Statistics 25.0. One-way analysis of variance (ANOVA) followed by Duncan's multiple range test was employed to evaluate differences among groups. A p-value of < 0.05 or < 0.01 was considered statistically significant.

Results

Chemical Composition Analysis

The linear regression equation describing the relationship between anhydrous glucose

concentration (C) and absorbance (A) was A=0.051C−0.0099(r=0.999), demonstrating excellent linearity over the concentration range of 4.41~15.86μg/mL and satisfying the requirements for quantitative analysis. The linear regression equation for Fe^{2+} concentration versus absorbance was A = 0.2066x + 0.0097(r=0.999), indicating a strong linear relationship within the concentration range of 0.8~4.0 μg/mL. Similarly, the calibration curve for protein determination yielded the equation A = 9.9057x + 0.0124 (r = 0.9998), exhibiting excellent linearity over the concentration range of 0.02~0.10 mg/mL.

As shown in Table 10, the neutral sugar and protein contents of APS were 82.15 ± 5.53% and 1.23 ± 0.87%, respectively. Following complexation with iron, the neutral sugar and protein contents decreased to 75.32 ± 4.28% and 0.94 ± 0.74%, respectively, in the APS-iron(II) complex, and to 73.25 ± 5.38% and 0.96 ± 0.56%, respectively, in the APS-iron(III) complex.

The reduction in neutral sugar content may be attributed to the coordination of iron ions with polysaccharide chains, which enhances the resistance of the glycosidic structures to hydrolysis and consequently results in a lower apparent neutral sugar content[23]. The decrease in protein content is likely associated with protein denaturation under the relatively harsh reaction conditions employed during complex synthesis, followed by the removal of denatured proteins through repeated centrifugation and purification procedures.

Tab.1 Chemical Composition Results

	APS	APS-iron (II)	APS-iron (III)
Neutral sugars/%	82.15±5.53	75.32±4.28	73.25±5.38
protein/%	1.23±0.87	0.94±0.74	0.96±0.56

As presented in Table 11, the iron content of the APS-iron(II) complex was 35.64 ± 3.64%, whereas that of the APS-iron(III) complex was 31.53 ± 4.67%. These results indicate that APS is capable of effectively coordinating with both Fe^{2+} and Fe^{3+} ions to form stable polysaccharide-iron complexes. Notably, the APS-iron(II) complex exhibited a higher iron content than the APS-iron(III) complex, suggesting a greater binding affinity of APS toward Fe^{2+}. This enhanced interaction may facilitate the formation of a more compact and stable complex structure, thereby resulting in a higher iron-loading capacity.

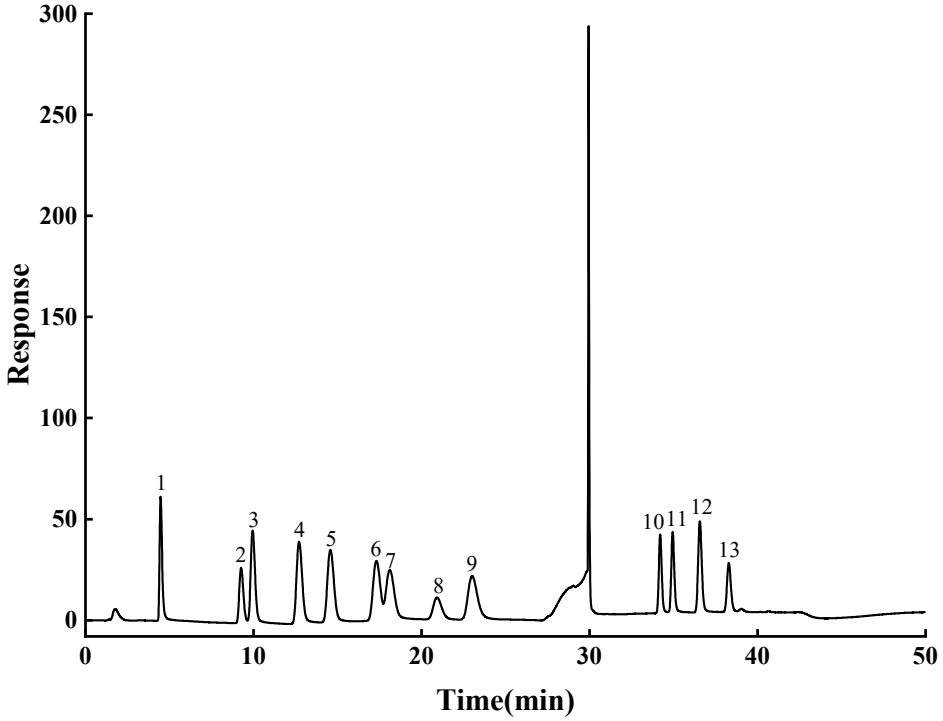
Tab.2 Iron content results

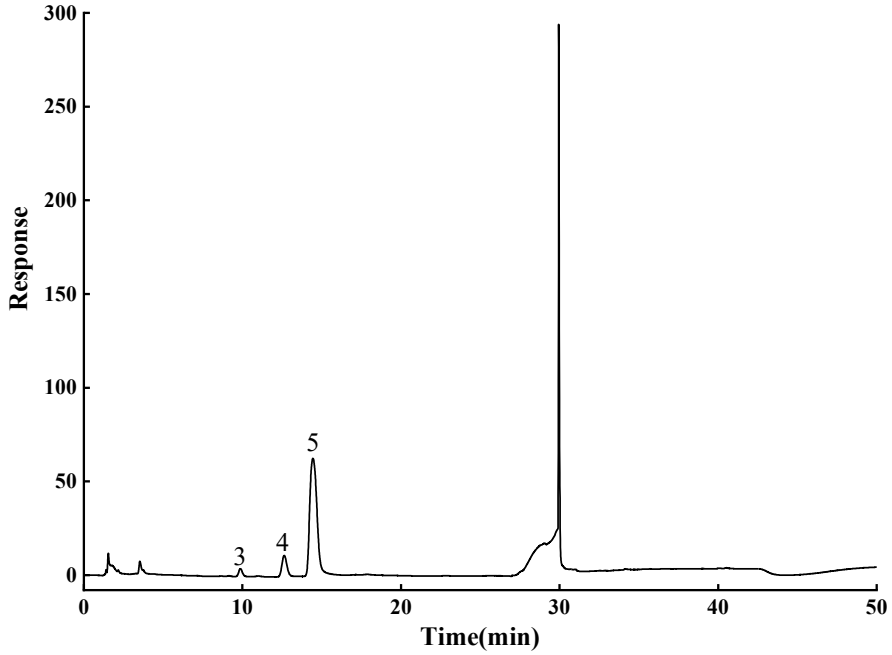
	APS-iron (II)	APS-iron (III)
Fe Content/%	35.64±3.64	31.53±4.67

Tab.3 Monosaccharide standard curve results

Name	appearance time	linear equation	r	linearity range（μg/mL）
Fuc	4.475	y =0.562x+0.4115	0.9979	0.4-24
Rha	9.259	y=0.376x+0.2895	0.9978	0.4-24
Ara	9.950	y=0.6966x+0.3557	0.9987	0.4-24
Gal	12.709	y=0.7852x+0.5457	0.9968	0.4-24
Glc	14.575	y=0.7873x+0.6152	0.9971	0.4-24
Xyl	17.317	y=0.7406x+0.4990	0.9976	0.4-20
Man	18.117	y=0.5821x+0.4781	0.9987	0.5-30

Fru	20.925	y=0.2041x+0.1903	0.9993	0.6-36
Rib	23.009	y=0.5042x+0.1959	0.9992	0.6-36
Gal-UA	34.209	y=0.2638x+0.1007	0.9996	0.6-36
Gul-UA	34.950	y=0.2854x+0.0907	0.9995	0.6-36
Glc-UA	36.567	y=0.3816x+0.2808	0.9992	0.6-36
Man-UA	38.284	y=0.2124x+0.1003	0.9997	0.6-36





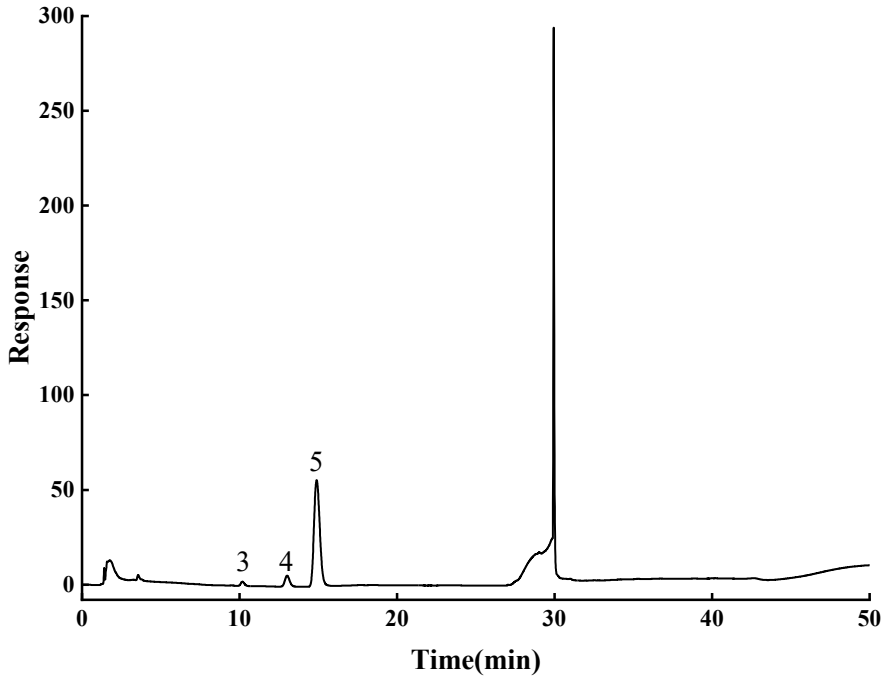


Fig 1 Chromatogram of monosaccharide composition

A: Chromatogram of the monosaccharide reference standards; B: Chromatogram of the APS sample; C: Chromatogram of the APS-iron(II) complex sample.

1-Fuc；2-Rha；3-Ara；4-Gal；5-Glc；6-Xyl；7-Man；8-Fru；9-Rib；10-Gal-UA；11-Gul-UA；12-Glc-UA；13-Man-UA

Tab 4 Changes in monosaccharides before and after APS synthesis of ferrous iron

	Ara	Gal	Glc
APS（μg/mL）	1.6207	5.1394	40.9771
APS-iron(II)（μg/mL）	0.8212	2.5256	29.2524

Therapeutic effects of the APS-iron(II) Complex in rats with iron-deficiency anemia

Effect of the APS-iron(II) Complex on Growth and Development in IDA Rats

Rats with IDA exhibited pale ears, hair loss, and reduced social interaction as a consequence of prolonged iron deficiency and repeated blood loss. Following treatment, rats receiving polysaccharide-iron complex capsules (PIC), ferrous succinate, or low-, medium-, and high-dose APS-iron(II) showed recovery of pink ear coloration, smoother fur, and improved social behavior. Changes in body weight are shown in the corresponding figure. During the 2~4-week model induction period, the body weights of IDA rats were consistently lower than those of the normal control group. After treatment, the high-dose APS-iron(II) group exhibited body weight recovery to levels comparable with those of the normal controls. The medium-dose APS-iron(II) group showed a greater recovery than the other treatment groups but remained below the normal control and high-dose groups. The low-dose APS-iron(II), ferrous succinate, PIC, and APS-iron(III) groups displayed broadly similar improvements in body weight, all of which exceeded those observed in the untreated IDA model group and the APS-only group.

In contrast, the APS-only group demonstrated relatively poor body weight recovery, and its final body weight remained close to that of the untreated IDA model group. These findings suggest that APS administered alone was insufficient to reverse the body weight loss associated with IDA in this model, whereas iron-containing APS complexes, particularly the high-dose APS-iron(II)

formulation, produced a more pronounced restorative effect on growth and development.

Tab 5 Weight Change in Rats($\bar{x}\pm s$，n=8)

Week	0	1	2	3	4	5	6	7	8	9
BG	155.08 ±4.94	186.40 ±9.11	214.59± 14.19	242.62± 14.22	257.57± 13.11	272.26± 17.21	285.91± 16.86	294.89± 17.79	305.59± 19.14	310.46±13.46***
IDA	151.97 ±2.26	169.47 ±8.75	192.19± 11.28	209.89± 11.64	220.01± 13.06	228.79± 14.49	238.65± 18.43	243.55± 13.49	249.10± 18.69	250.54±19.64###
FS	156.01 ±2.47	180.74 ±4.62	204.25± 7.08	220.60± 9.29	232.87± 11.47	247.62± 11.14	256.46± 10.99	262.62± 13.82	270.56± 16.14	274.86±9.93##*
PIC	151.32 ±2.19	175.20 ±6.60	195.35± 8.26	218.81± 14.16	227.22± 12.66	240.46± 15.99	247.03± 15.84	252.75± 15.27	267.47± 10.85	273.00±17.11##*
APS	149.27 ±1.24	173.65 ±5.12	195.85± 8.47	211.83± 8.59	221.21± 6.81	228.50± 6.40	239.32± 9.54	249.46± 14.44	251.84± 13.63	251.89±10.43###
APS-iron (III)	150.93 ±4.68	175.58 ±10.52	195.28± 11.78	217.29± 13.46	228.70± 13.94	242.34± 14.97	244.00± 15.94	257.82± 17.48	261.57± 19.31	271.27±21.91###*
L-APS-iron (II)	150.37 ±4.38	179.59 ±2.46	201.98± 5.42	222.39± 13.07	237.45± 18.90	241.13± 15.30	257.94± 13.31	263.82± 15.95	270.51± 17.10	274.59±17.90##*
M-APS-iron (II)	149.27 ±3.27	171.71 ±5.02	190.99± 3.92	200.54± 8.32	228.60± 11.47	243.29± 6.76	262.46± 12.14	275.25± 8.36	286.78± 7.42	297.73±10.43***
H-APS-iron (II)	149.14 ±3.51	172.79 ±3.89	192.29± 8.01	222.81± 6.51	234.77± 6.75	256.50± 11.72	268.43± 12.33	284.18± 14.40	292.28± 12.76	305.90±13.69***

Note: # indicates a significant difference compared with the blank control group ($p < 0.05$); ## indicates a highly significant difference compared with the blank control group ($p < 0.01$); ### indicates an extremely significant difference compared with the blank control group ($p < 0.001$). * indicates a significant difference compared with the model group ($p < 0.05$); ** indicates a highly significant difference compared with the model group ($p < 0.01$); and *** indicates an extremely significant difference compared with the model group ($p < 0.001$).

Effects of APS-Iron(II) Complex on Erythrocyte Parameters in Rats with Iron-Deficiency Anemia. The erythrocyte parameters of rats in each group were evaluated after successful establishment of the IDA model and 4 weeks of treatment. The results are presented in Table 6. Compared with the normal control group, the model group exhibited significantly reduced erythrocyte parameters ($p < 0.05$), confirming the successful establishment of the IDA model.

Compared with the model group, all treatment groups, including the positive control groups and APS-treated groups, showed significantly improved erythrocyte parameters ($p < 0.05$). Relative to the normal control group, no significant differences were observed in HGB, MCH, and MCHC values in the low-dose APS-iron(II) group and the APS-iron(III) group, nor in RBC and HCT values in the high-dose APS-iron(II) group. In addition, MCV values in all treatment groups were not significantly different from those of the normal control group. Notably, the medium- and high-dose APS-iron(II) groups exhibited significantly higher HGB, MCH, and MCHC values than the normal control group ($p < 0.05$).

When compared with the polysaccharide-iron complex capsule (PIC) group, the medium- and high-dose APS-iron(II) groups demonstrated significantly higher HGB levels, while the high-dose APS-iron(II) group also showed significantly elevated RBC and HCT values ($p < 0.05$). Similarly, relative to the ferrous succinate group, the medium- and high-dose APS-iron(II) groups exhibited significantly increased HGB and MCHC levels, and the high-dose group showed significantly higher RBC and HCT values ($p < 0.05$). Furthermore, compared with the APS-iron(III) group, the medium- and high-dose APS-iron(II) groups displayed significantly greater HGB and MCHC values, whereas the high-dose APS-iron(II) group exhibited significantly higher RBC, HCT, and MCH levels ($p < 0.05$).

Collectively, these findings indicate that the medium- and high-dose APS-iron(II) complexes were more effective in restoring erythrocyte parameters in IDA rats than the three positive control treatments, namely PIC, ferrous succinate, and APS-iron(III). In contrast, administration of APS alone resulted in significantly weaker improvements in erythrocyte parameters compared with APS-iron(II) complexes and the positive control groups ($p < 0.05$). These results suggest that complexation of APS with Fe^{2+} markedly enhances its hematopoietic activity and therapeutic efficacy against iron-deficiency anemia.

Tab 6 Erythrocyte parameters in rats of different groups($\bar{x} \pm s$，n=8)

	HGB	RBC	HCT	MCV	MCH	MCHC
BG	145.37±3.24^{c}	8.50±0.36^{e}	45.77±1.52^{e}	53.85±1.38^{bc}	17.11±0.73^{b}	31.78±1.04^{b}
IDA	93.00±4.14^{a}	6.41±0.22^{a}	32.38±0.83^{a}	50.51±1.30^{a}	14.50±0.59^{a}	28.72±1.29^{a}
PIC	143.87±6.24^{c}	8.00±0.29^{c}	43.26±1.17^{cd}	54.08±2.13^{bc}	17.98±0.94^{bcd}	33.27±1.67^{cd}
FS	142.00±4.78^{c}	7.92±0.14^{c}	43.06±0.75^{cd}	54.37±1.34^{bc}	17.93±0.67^{bcd}	32.98±1.10^{bc}
APS	105.38±5.68^{b}	7.02±0.14^{b}	36.02±1.29^{b}	51.35±2.36^{ab}	15.01±0.72^{a}	29.27±1.58^{a}
APS-iron (III)	141.75±4.56^{c}	8.00±0.30^{c}	43.42±0.76^{cd}	54.37±2.81^{bc}	17.75±1.10^{bc}	32.65±1.09^{bc}
L-APS-iron (II)	141.12±3.52^{c}	7.94±0.21^{c}	42.99±0.83^{c}	54.13±1.39^{bc}	17.76±0.51^{bc}	32.83±0.91^{bc}
M-APS-iron (II)	152.58±3.21^{d}	8.11±0.22^{cd}	44.32±1.08^{d}	54.66±2.37^{c}	18.81±0.75^{cd}	34.44±1.01^{d}
H-APS-iron (II)	158.12±5.33^{d}	8.35±0.17^{de}	45.73±1.76^{e}	54.75±2.05^{c}	18.92±0.60^{d}	34.61±1.78^{d}

No significant difference was found between the same lowercase letters in the same column; however, significant differences were observed between different lowercase letters (P<0.05).

Changes in Serum Iron Levels in Rats

After successful establishment of the IDA model and 4 weeks of treatment, changes in serum iron parameters were evaluated, and the results are presented in Table 7. Compared with the normal control group, the model group exhibited significantly decreased serum iron (SI) and transferrin saturation (TSAT), along with a marked increase in total iron-binding capacity (TIBC) ($p < 0.05$). Compared with the model group, all treatment groups, including the positive control and APS-treated groups, showed significantly increased SI and TSAT levels and significantly reduced TIBC values ($p < 0.05$). Relative to the normal control group, SI in the low-, medium-, and high-dose APS-iron(II) groups showed no significant differences. TSAT in the low- and medium-dose APS-iron(II) groups was also comparable to that of the normal control group, whereas the high-dose APS-iron(II) group exhibited significantly higher TSAT levels ($p < 0.05$). In addition, TIBC values in all APS-iron(II) dose groups were significantly lower than those in the normal control group ($p < 0.05$), while no significant difference in TIBC was observed in the APS-iron(III) group.

Compared with the positive control groups, the low-, medium-, and high-dose APS-iron(II) groups showed significantly higher SI and TSAT levels ($p < 0.05$). TIBC values in all APS-iron(II) dose groups were significantly lower than those in the polysaccharide-iron complex capsule (PIC) group ($p < 0.05$), while the high-dose APS-iron(II) group also showed significantly lower TIBC compared with the ferrous succinate group ($p < 0.05$). Moreover, compared with the APS-iron(III) group, all APS-iron(II) dose groups exhibited significantly higher SI and TSAT levels and significantly lower TIBC values ($p < 0.05$).

Iron deficiency is typically accompanied by a significant reduction in SI levels, which in turn stimulates compensatory upregulation of renal erythropoietin (EPO) secretion[24]. As shown in Table 7, EPO levels in the model group were significantly higher than those in the normal control group ($p < 0.05$). After treatment, the medium-dose APS-iron(II) group exhibited significantly lower EPO levels than the PIC group, while the high-dose APS-iron(II) group showed significantly reduced EPO levels compared with both the ferrous succinate and PIC groups ($p < 0.05$).

These changes in downstream iron metabolism markers, particularly EPO, suggest that all doses of APS-iron(II) complexes significantly improved iron absorption and utilization efficiency in IDA rats. Notably, their effects were superior to those of ferrous succinate, PIC, and APS-iron(III), indicating that the APS-iron(II) complex exhibits enhanced regulatory efficacy in promoting iron metabolism.

Table 7 Analysis of iron content changes in serum of different groups of rats($\bar{x} \pm s$, n=8)

Group	SI/μmol	TIBC/μmol/L	TSAT/%	EPO/（mIU/mL）
BG	61.05±3.60^{e}	126.52±3.25^{cd}	48.28±3.08^{e}	27.84±1.89^{d}
IDA	25.67±2.65^{a}	215.32±6.30^{a}	11.93±1.22^{a}	43.96±2.20^{a}
PIC	51.50±1.96^{d}	134.52±7.76^{c}	38.46±3.56^{cd}	35.74±3.87^{b}
FS	41.98±2.88^{c}	120.42±4.33^{de}	34.90±2.64^{c}	34.80±1.80^{bc}
APS	30.89±2.25^{b}	128.75±8.49^{b}	17.78±1.33^{b}	40.38±1.24^{a}
APS-iron（III）	53.30±1.57^{d}	173.80±2.43^{c}	41.55±2.98^{d}	31.26±2.95^{cd}
L-APS-iron（II）	58.65±3.57^{e}	118.03±5.93^{e}	49.83±4.41^{e}	36.93±3.07^{b}
M-APS-iron（II）	60.60±3.01^{e}	117.30±6.11^{e}	51.77±3.36^{e}	32.26±2.38^{c}
H-APS-iron（II）	61.11±3.40^{e}	108.13±5.92^{f}	56.71±5.03^{f}	28.05±2.08^{d}

No significant difference was found between the same lowercase letters in the same column; however, significant differences were observed between different lowercase letters (P<0.05).

Organ Index Results in Rats

Organ indices are commonly used as indicators of drug safety for evaluating potential toxicity[25]. As shown in Table 8, compared with the normal control group, the model group exhibited significantly increased heart and spleen indices ($p < 0.05$) and significantly decreased liver and kidney indices ($p < 0.05$), indicating successful establishment of the IDA model.

Compared with the normal control group, in the APS-iron(II) treatment groups, the spleen index was significantly lower across all doses ($p < 0.05$), while the kidney index in the high-dose APS-iron(II) group was significantly higher than that of the normal control group ($p < 0.05$).

Compared with the ferrous succinate group, the medium- and high-dose APS-iron(II) groups showed significantly lower heart indices ($p < 0.05$), whereas the high-dose APS-iron(II) group exhibited a significantly higher kidney index ($p < 0.05$). Relative to the ferrous succinate group, the high-dose APS-iron(II) group also showed a significantly higher liver index($p < 0.05$), while the medium-dose group exhibited a significantly lower heart index ($p < 0.05$). In addition, the high-dose APS-iron(II) group presented a significantly higher kidney index than the APS-iron(III) group ($p < 0.05$).

Overall, these findings suggest that, compared with the positive control groups, the APS-iron(II) complex exerts a more favorable modulatory effect on organ indices in IDA rats, indicating a potentially improved safety and physiological recovery profile.

Tab 8 Analysis Results of Organ Index in Different Rat Groups($\bar{x}\pm s$，n=8)

	liver	spleen	heart	kidney
BG	3.22 ± 0.05^{cd}	0.27 ± 0.01^{b}	0.32 ± 0.01^{cde}	0.63 ± 0.02^{bc}
IDA	2.61 ± 0.24^{a}	0.31 ± 0.02^{a}	0.43 ± 0.01^{a}	0.55 ± 0.02^{a}
PIC	3.13 ± 0.06^{cd}	0.24 ± 0.02^{c}	0.34 ± 0.01^{c}	0.62 ± 0.02^{bc}
FS	3.10 ± 0.06^{c}	0.25 ± 0.02^{bc}	0.33 ± 0.02^{cd}	0.65 ± 0.02^{cd}
APS	2.90 ± 0.14^{b}	0.30 ± 0.02^{a}	0.40 ± 0.02^{b}	0.57 ± 0.03^{a}
APS-iron(III)	3.23 ± 0.16^{cd}	0.23 ± 0.02^{c}	0.32 ± 0.03^{de}	0.62 ± 0.04^{bc}
L-APS-iron(II)	3.15 ± 0.22^{cd}	0.24 ± 0.03^{c}	0.33 ± 0.03^{cde}	0.61 ± 0.04^{b}
M-APS-iron(II)	3.26 ± 0.11^{cd}	0.23 ± 0.04^{c}	0.31 ± 0.02^{e}	0.64 ± 0.03^{bcd}
H-APS-iron(II)	3.32 ± 0.10^{d}	0.22 ± 0.02^{c}	0.32 ± 0.03^{de}	0.66 ± 0.03^{d}

No significant difference was found between the same lowercase letters in the same column; however, significant differences were observed between different lowercase letters (P<0.05).

Serum Antioxidant Enzyme Activities in Different Experimental Groups

As shown in Table 9, compared with the normal control group, the model group exhibited a significant increase in serum malondialdehyde (MDA) levels ($p < 0.05$), accompanied by significant decreases in glutathione peroxidase (GSH-Px), catalase (CAT), and superoxide dismutase (SOD) activities ($p < 0.05$), indicating the presence of oxidative stress in IDA rats.

Compared with the model group, all treatment groups except the APS-only group showed significantly reduced MDA levels ($p < 0.05$) and significantly increased activities of GSH-Px, CAT, and SOD ($p < 0.05$). Relative to the normal control group, no significant differences were

observed in MDA, GSH-Px, and SOD levels in the APS-iron(II) and APS-iron(III) groups, suggesting a near-normalization of these oxidative stress markers.

Compared with the positive control groups (ferrous succinate and PIC), the high-dose APS-iron(II) and APS-iron(III) groups exhibited significantly lower MDA levels ($p < 0.05$) and significantly higher GSH-Px and CAT activities ($p < 0.05$), while SOD activity in the high-dose APS-iron(II) group was significantly higher than that in the positive control groups ($p < 0.05$).

In the APS-only group, MDA levels showed no significant difference compared with the model group, whereas GSH-Px, CAT, and SOD activities were significantly increased compared with the model group ($p < 0.05$), but remained significantly lower than those in the other treatment groups ($p < 0.05$).

Collectively, these results indicate that medium- and high-dose APS-iron(II) complexes exert superior antioxidative stress effects in IDA rats compared with ferrous succinate, polysaccharide-iron complex capsules, and the APS-iron(III) complex. Moreover, APS alone also exhibits a certain degree of antioxidant activity in IDA rats, albeit with comparatively weaker efficacy.

Tab 9 Serum Antioxidase Activity Results in Different Rat Groups($\bar{x}\pm s$，n=6)

分组	MDA	GSH-Px	CAT	SOD
BG	3.52 ± 0.17^{c}	397.31 ± 16.26^{d}	69.47 ± 3.63^{f}	169.03 ± 9.89^{e}
IDA	6.14 ± 0.27^{a}	244.56 ± 17.88^{a}	31.33 ± 1.71^{a}	99.72 ± 13.82^{a}
PIC	4.42 ± 0.81^{b}	329.54 ± 36.41^{bc}	56.54 ± 4.64^{d}	132.25 ± 11.09^{bc}
FS	4.43 ± 0.26^{b}	340.48 ± 22.27^{c}	49.74 ± 3.71^{c}	144.88 ± 10.90^{cd}
APS	5.91 ± 0.47^{a}	299.06 ± 19.40^{b}	40.58 ± 1.60^{b}	117.66 ± 9.84^{b}
APS-iron（III）	3.74 ± 0.36^{c}	386.83 ± 19.82^{d}	62.18 ± 4.61^{e}	152.84 ± 13.22^{de}
L-APS-iron（II）	4.61 ± 0.36^{b}	322.03 ± 13.54^{bc}	45.14 ± 3.95^{c}	143.28 ± 5.80^{cd}
M-APS-iron（II）	3.82 ± 0.28^{c}	349.93 ± 11.09^{c}	52.99 ± 4.41^{d}	152.47 ± 6.49^{de}
H-APS-iron（II）	3.69 ± 0.18^{c}	396.33 ± 13.78^{d}	63.06 ± 3.11^{e}	160.70 ± 9.90^{e}

No significant difference was found between the same lowercase letters in the same column; however, significant differences were observed between different lowercase letters (P<0.05).

Hepatic Antioxidant Enzyme Activities in Different Experimental Groups

As shown in Table 10, compared with the normal control group, the model group exhibited a significant increase in hepatic malondialdehyde (MDA) levels ($p < 0.05$), accompanied by significant decreases in glutathione peroxidase (GSH-Px), catalase (CAT), and superoxide dismutase (SOD) activities ($p < 0.05$), indicating pronounced oxidative stress in the liver of IDA rats.

Compared with the model group, all treatment groups except the APS-only group showed significantly reduced MDA levels ($p < 0.05$) and significantly increased activities of GSH-Px, CAT, and SOD ($p < 0.05$). Relative to the normal control group, no significant differences were observed in MDA and GSH-Px levels in the APS-iron(II) and APS-iron(III) groups. In addition, CAT and SOD activities in the APS-iron(II) group were comparable to those of the normal control group.

Compared with the positive control groups (ferrous succinate and PIC), both the APS-iron(II) and APS-iron(III) groups exhibited significantly lower MDA levels ($p < 0.05$) and significantly higher GSH-Px and CAT activities ($p < 0.05$), while SOD activity in the APS-iron(II) group was

significantly higher than that in the positive control groups ($p < 0.05$).
Furthermore, compared with the APS-iron(III) group, the APS-iron(II) group showed significantly lower MDA levels ($p < 0.05$) and significantly higher CAT and SOD activities ($p < 0.05$).
In the APS-only group, MDA levels showed no significant difference compared with the model group, whereas GSH-Px, CAT, and SOD activities were significantly higher than those in the model group ($p < 0.05$), but remained significantly lower than those in the other treatment groups.
Collectively, these findings demonstrate that APS-iron(II) exerts superior protective effects against hepatic oxidative stress in IDA rats compared with ferrous succinate, polysaccharide-iron complex capsules, and APS-iron(III). In contrast, APS alone shows limited efficacy in ameliorating hepatic oxidative stress under IDA conditions.

Tab 10 Results of Antioxidant Enzyme Activities in Liver of Different Groups of Rats($\bar{x}\pm s$，n=6)

分组	MDA/（nmol/g）	GSH-Px/（U/mL）	CAT/（U/mL）	SOD/（U/mL）
BG	43.92±4.81^{de}	475.51±18.98^{d}	77.82±3.78^{f}	193.96±7.70^{e}
IDA	66.28±4.71^{a}	248.02±18.07^{a}	36.55±2.96^{a}	86.20±4.37^{a}
PIC	58.09±1.74^{bc}	370.61±19.44^{c}	63.59±3.11^{d}	164.56±13.75^{d}
FS	55.27±4.89^{c}	393.30±9.40^{c}	54.34±2.69^{c}	137.99±13.28^{c}
APS	62.51±1.35^{ab}	329.21±19.76^{b}	46.97±7.55^{b}	113.36±8.14^{b}
APS-iron（III）	48.27±5.54^{d}	465.90±20.38^{d}	71.64±2.66^{e}	139.26±10.15^{c}
L-APS-iron（II）	52.81±5.62^{c}	384.91±15.25^{c}	50.66±5.20^{bc}	133.17±6.66^{c}
M-APS-iron（II）	47.43±3.81^{d}	470.43±18.68^{d}	64.53±8.58^{d}	167.62±15.90^{d}
H-APS-iron（II）	41.02±1.88^{e}	482.82±12.74^{d}	78.65±3.75^{f}	195.19±12.27^{e}

No significant difference was found between the same lowercase letters in the same column; however, significant differences were observed between different lowercase letters (P<0.05).

Histopathological Analysis of Rat Liver Tissue

As illustrated in Figure 6, hematoxylin and eosin (H&E) staining of liver sections from the normal control group revealed a well-preserved hepatic architecture. The hepatic capsule consisted of uniformly thick dense connective tissue rich in elastic fibers. The central vein was located in the center of each hepatic lobule and was surrounded by radially arranged hepatocytes and hepatic sinusoids (gray arrows). The hepatic cords (light green arrows) were regularly organized and clearly defined. No hepatocellular vacuolar degeneration or obvious inflammatory cell infiltration was observed.
In contrast, liver sections from the model group exhibited marked histopathological abnormalities. Hepatic sinusoids were irregularly arranged, and the boundaries of the hepatic cords were indistinct. Extensive hepatocellular vacuolar degeneration (blue arrows), characterized by the presence of small cytoplasmic vacuoles, was observed. In addition, widespread hydropic degeneration of hepatocytes (green arrows) was evident, as indicated by pale, loosely stained cytoplasm and cellular swelling. Focal infiltration of lymphocytes and granulocytes was detected around blood vessels (yellow arrows), accompanied by vascular congestion and extensive sinusoidal congestion (red arrows).
Treatment with the medium-dose APS-iron(II) complex and APS alone markedly reduced the extent of hepatocellular vacuolar degeneration (blue arrows) and hydropic degeneration (green arrows). Furthermore, the architecture of hepatic cords and sinusoids became more organized, and

no obvious inflammatory cell infiltration was observed. In contrast, focal infiltration of lymphocytes and granulocytes (yellow arrows) remained evident in the APS-iron(III) group.

These histopathological improvements suggest that the Astragalus polysaccharide component effectively scavenged reactive oxygen species (ROS), thereby mitigating oxidative damage and preserving the structural integrity of hepatocytes. Such findings are consistent with the enhanced antioxidant activity observed following APS-based treatment.

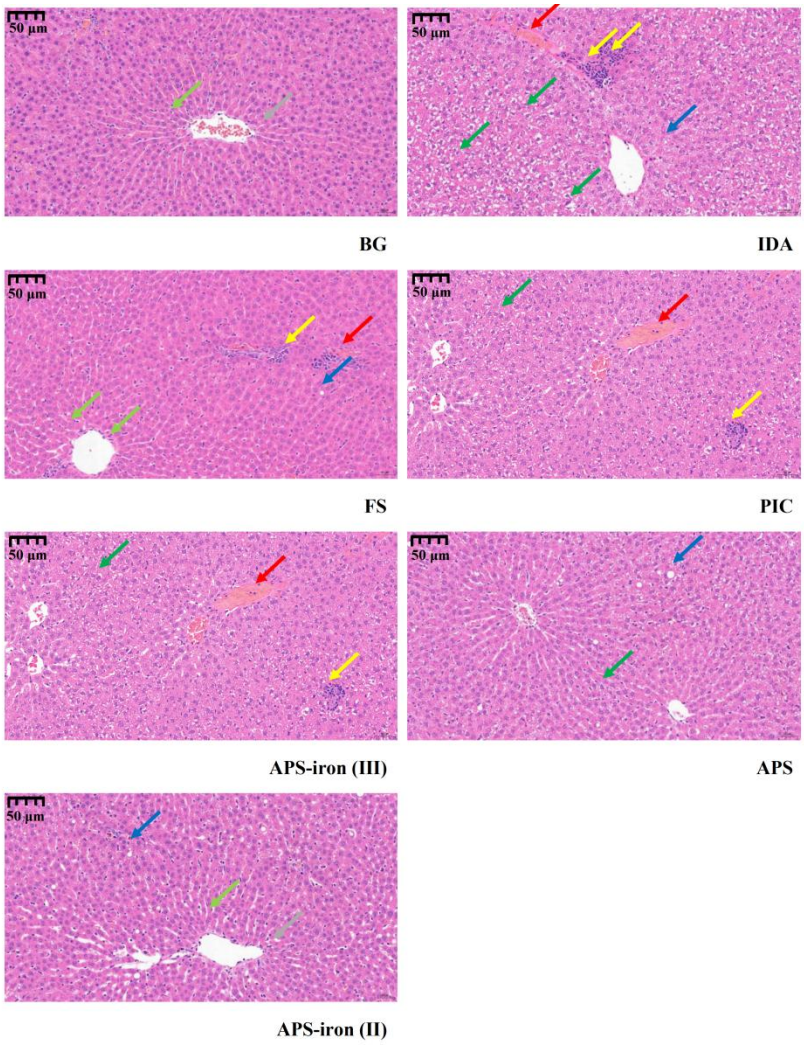


Fig 6 HE staining of rat liver（20.0 x）

Note: Gray arrows indicate hepatic sinusoids; light green arrows indicate hepatic cords; blue arrows indicate hepatocellular vacuolar degeneration; green arrows indicate hydropic degeneration; yellow arrows indicate focal infiltration of lymphocytes and granulocytes; and red arrows indicate sinusoidal congestion.

As shown in Figure 7, H&E staining of spleen tissues from the normal control group revealed a splenic capsule composed of dense connective tissue rich in elastic and smooth muscle fibers with a uniform thickness. Trabeculae extended from the capsule into the splenic parenchyma, and no obvious histopathological abnormalities were observed. The splenic parenchyma consisted of red pulp, white pulp (black arrows), and the marginal zone. The white pulp was composed of periarteriolar lymphoid sheaths and lymphoid follicles surrounding the central arteries. The red pulp, distributed beneath the capsule, around the trabeculae, and external to the marginal zone of the white pulp, consisted primarily of splenic cords (gray arrows) and splenic sinusoids (light

green arrows). In contrast, spleen sections from the model group exhibited abundant macrophages within the red pulp (orange arrows), granulocytic infiltration (yellow arrows), and marked splenic sinusoidal congestion (red arrows).

As illustrated in Figure 8, H&E staining of kidney tissues from the normal control group demonstrated a normal renal architecture, characterized by a uniform distribution of glomerular cells and mesangial matrix, as well as rounded and intact tubular epithelial cells. In the model group, dilation of the Bowman's capsule (light green arrows) was observed. In addition, renal tubular epithelial cells exhibited vacuolar degeneration (blue arrows), characterized by the presence of small cytoplasmic vacuoles, along with mild hydropic degeneration (green arrows).

Following treatment, the medium-dose APS-iron(II) group exhibited the most pronounced histopathological improvement in both spleen and kidney tissues, with substantial restoration of normal tissue morphology and attenuation of pathological lesions. These findings further support the protective effects of APS-iron(II) against tissue injury associated with iron-deficiency anemia.

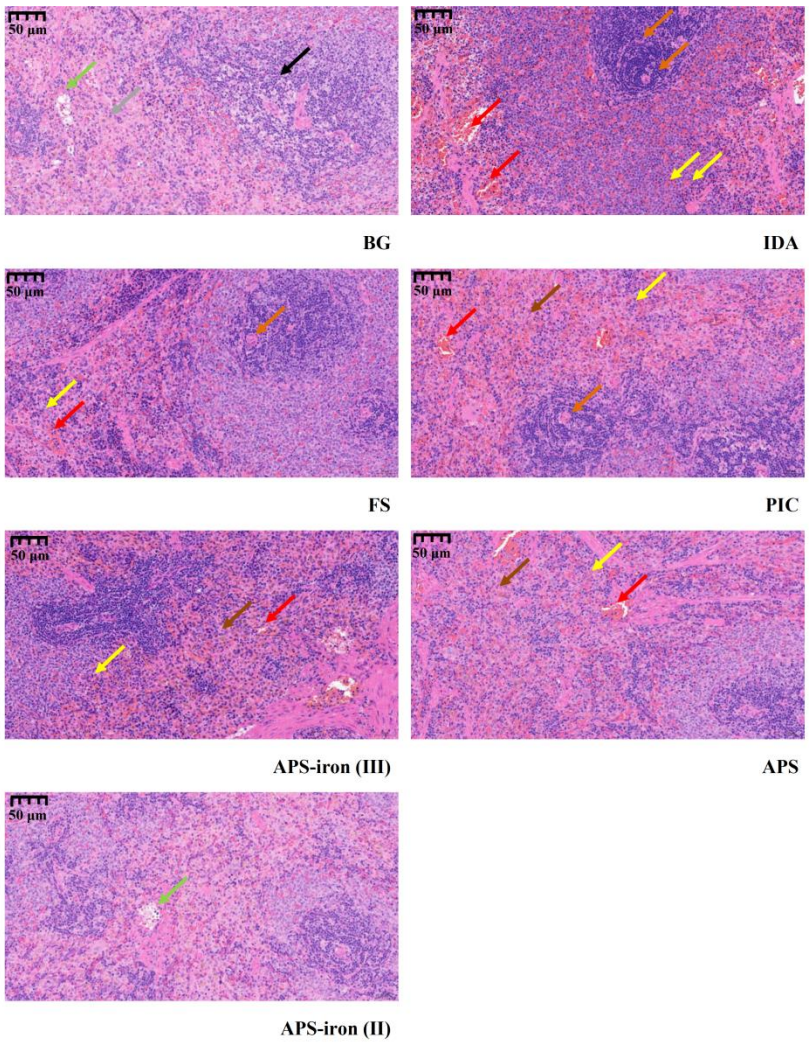


Fig 7 HE staining of rat spleen（20.0 x）

Note: Black arrows indicate the white pulp; gray arrows indicate the splenic cords; light green arrows indicate the splenic sinusoids; orange arrows indicate macrophages; yellow arrows indicate granulocytes; and red arrows indicate splenic sinusoidal congestion.

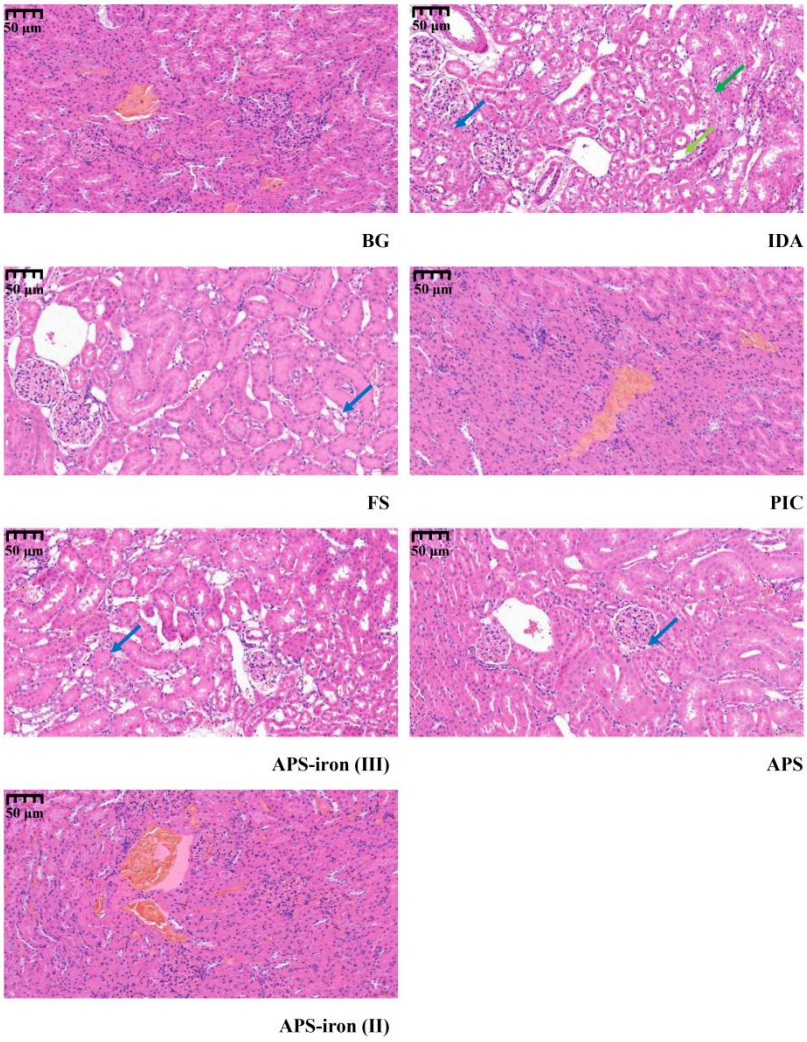


Fig 8 HE staining of rat kidneys（20.0 x）

Note: Light green arrows indicate dilatation of Bowman's capsule; blue arrows indicate cellular vacuolar degeneration; and green arrows indicate hydropic degeneration of cells.

Prussian blue staining was performed to evaluate iron distribution and storage in liver tissues. Iron-containing regions appeared blue, with staining intensity positively correlated with hepatic iron content[26]. As shown in Figure 9, only a small amount of brownish-yellow hemosiderin degradation products was observed in the normal control group, whereas no obvious blue staining was detected. In contrast, neither blue-stained iron deposits nor brownish-yellow iron metabolites were observed in the model group, indicating a severe depletion of hepatic iron stores.

Compared with the model group, both the ferrous succinate group and all treatment groups exhibited marked improvements, with substantially increased hepatic iron content. Notably, the APS-iron(II) group displayed a significantly larger area of blue iron-positive staining than the other groups, accompanied by more intense staining and the presence of moderate amounts of iron metabolites. These findings indicate superior restoration of hepatic iron reserves following APS-iron(II) administration.

Collectively, the results demonstrate that the APS-iron(II) complex is more effective than the control treatments in replenishing hepatic iron stores in IDA rats. Furthermore, the simultaneous presence of iron deposits and iron metabolic products suggests that APS-iron(II) not only

efficiently restores iron reserves but also maintains normal iron metabolism and utilization, thereby contributing to improved iron homeostasis.

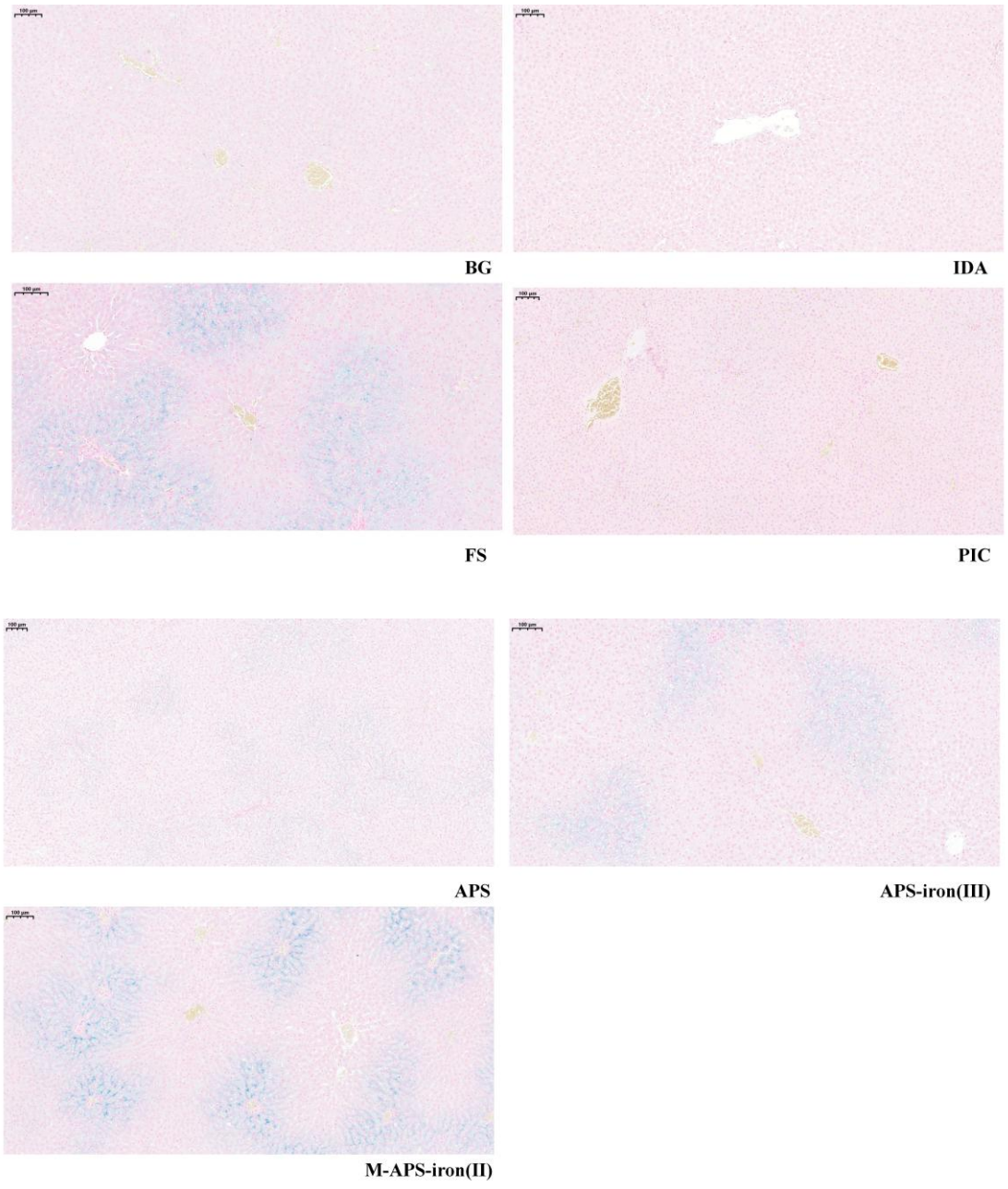


Fig 9 Prussian blue staining of rat liver

Effects of the APS-Iron(II) Complex on Gut Microbiota

Quality Control and Statistical Analysis of Gut Microbiota Sequencing Data

Both iron deficiency and iron overload can profoundly affect the composition, balance[27], and diversity of the gut microbiota. Sequences sharing ≥97% similarity were clustered into the same operational taxonomic units (OTUs). As illustrated in the Venn diagram (Figure 10), a total of 843 OTUs were identified across all samples. The normal control group (BG) possessed 266 unique OTUs, whereas the IDA group contained only 44 unique OTUs, indicating a substantial reduction in microbial richness following iron-deficiency anemia induction. In addition, 43 OTUs were shared among all experimental groups, representing the core microbial community.

As shown in Figure 11, the rarefaction curves gradually approached a plateau when the sequencing depth reached approximately 20,000 reads per sample, suggesting that the sequencing coverage was sufficient to capture the vast majority of microbial taxa present in the samples and that the sequencing depth met the requirements for subsequent diversity analyses.

Furthermore, the rank-abundance curves presented in Figure 12 exhibited smooth distributions, with the horizontal axis spanning a broad range and the vertical axis tending toward a plateau for all samples. These characteristics indicate a relatively high level of microbial richness and evenness within the communities. Collectively, these results demonstrate that the sequencing data were of adequate quality and depth to reliably characterize the richness, diversity, and community structure of the gut microbiota in each experimental group.

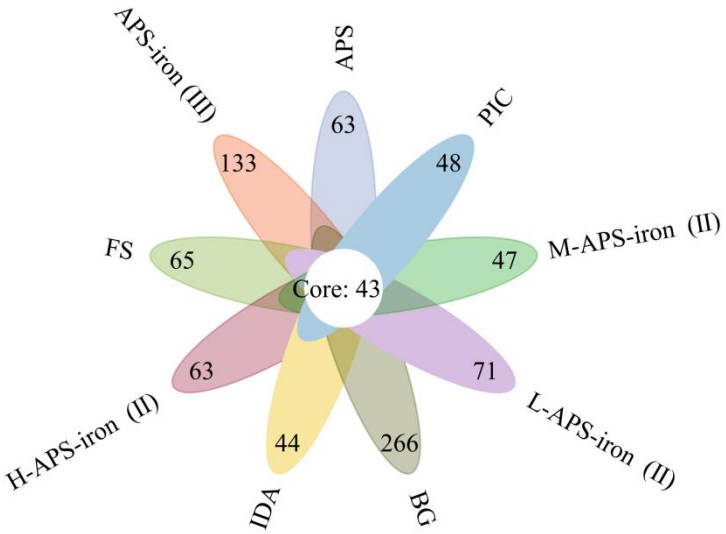


Fig 10 Feature Distribution Petal Chart

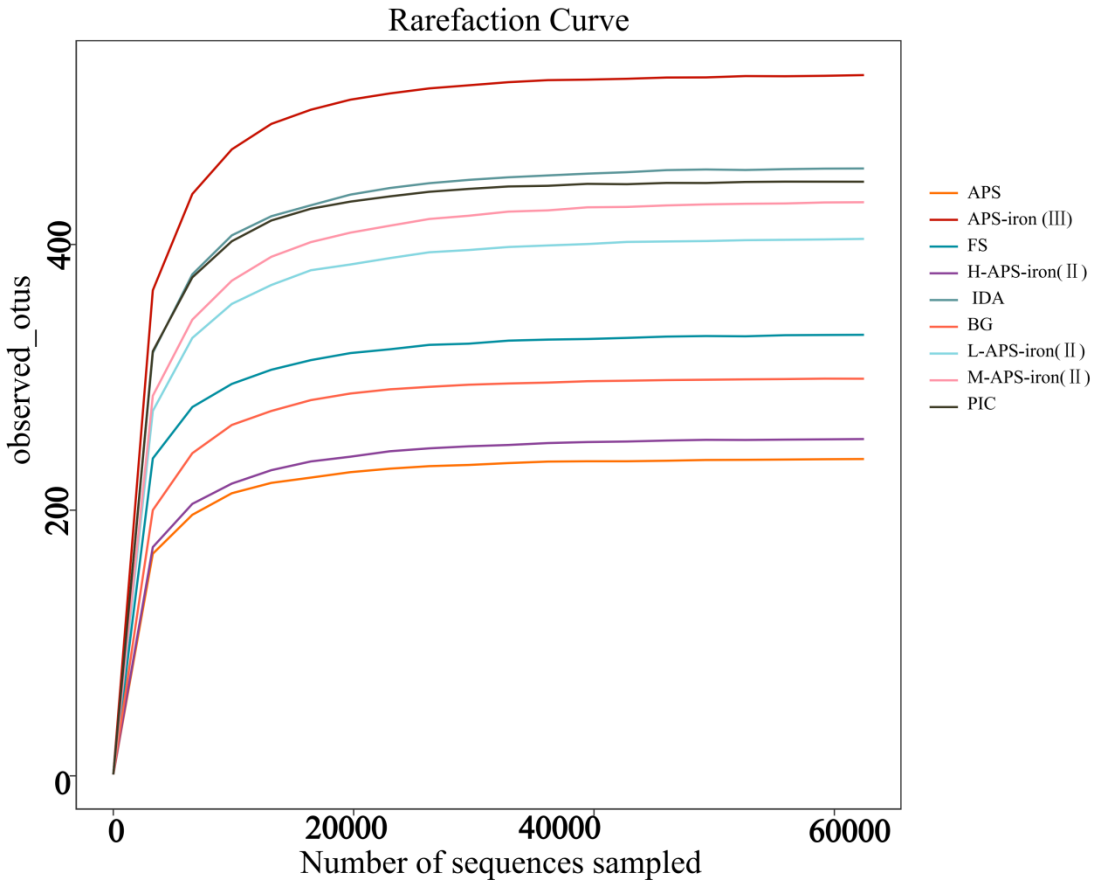


Fig 11 Sparse Curve

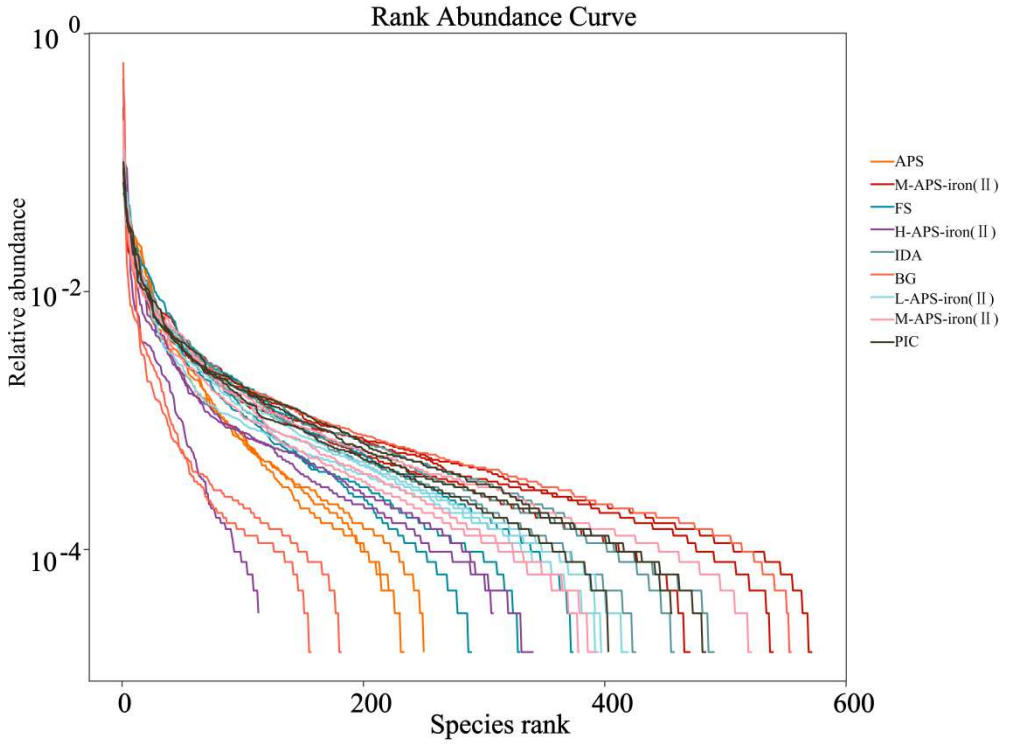


Fig 12 Hierarchical clustering curve

Effects of the APS-Iron(II) Complex on Gut Microbial Diversity

β-Diversity analysis was employed to evaluate differences in microbial community composition among the experimental groups. As shown in the hierarchical clustering dendrogram (Figure 13), two major branches were formed. The IDA model group, low- and medium-dose APS-iron(II) groups, PIC group, and APS-iron(III) group clustered together, whereas the normal control group, ferrous succinate group, APS group, and high-dose APS-iron(II) group formed a separate branch. This clustering pattern suggests that high-dose APS-iron(II) treatment restored the gut microbial community structure toward that observed in healthy animals.

The principal coordinates analysis (PCoA) plot (Figure 14) further demonstrated that the APS group and the high-dose APS-iron(II) group clustered more closely to the normal control group and were clearly separated from the IDA model group. These findings indicate that both treatments, particularly high-dose APS-iron(II), effectively ameliorated IDA-induced alterations in gut microbial composition.

As shown in Figure 15, the Ace, Chao1, and Shannon indices were used to evaluate microbial richness and diversity, with particular sensitivity to low-abundance taxa[28]. Compared with the normal control group, the IDA group exhibited significantly reduced Chao1, Ace, and Shannon indices, indicating a marked loss of microbial richness and diversity following iron-deficiency anemia induction. In contrast, the high-dose APS-iron(II) group and the PIC group displayed significantly increased Chao1, Ace, and Shannon indices, reflecting substantial restoration of gut microbial diversity.

Furthermore, the Simpson index in the high-dose APS-iron(II) group and the PIC group was significantly higher than that of the IDA model group, further supporting the recovery of microbial community complexity following treatment. Collectively, these results demonstrate that iron deficiency leads to a pronounced reduction in gut microbial richness and diversity, whereas intervention with the APS-iron(II) complex effectively restores microbial community structure and promotes the re-establishment of a healthier and more diverse gut microbiota.

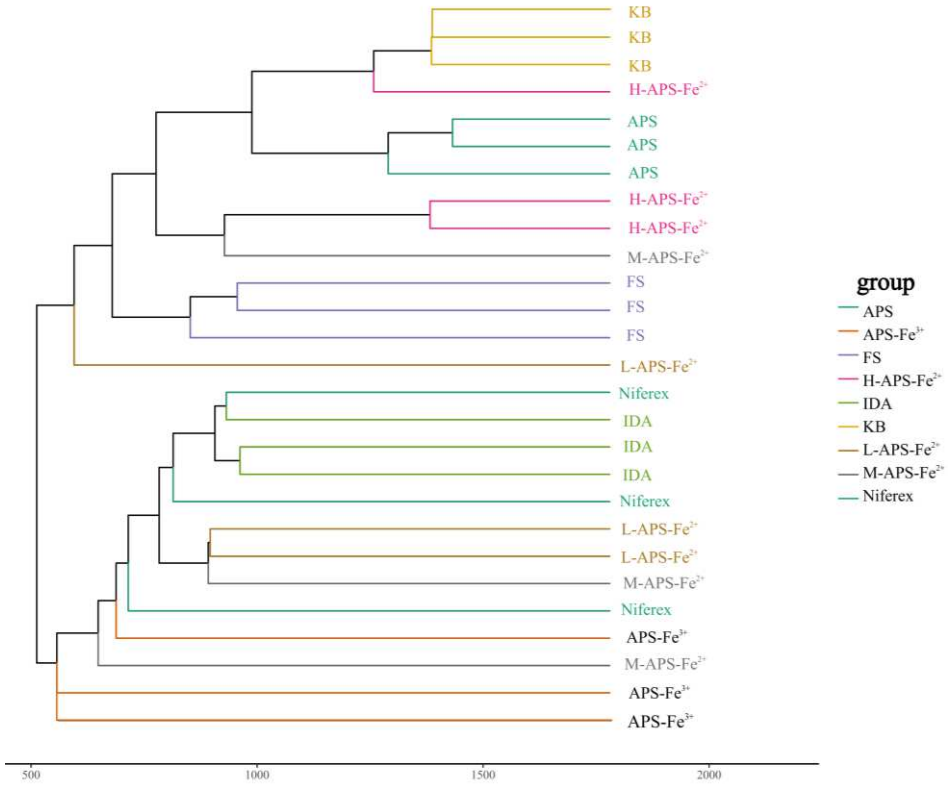


Fig 13 UPGMA Cluster Tree Diagram

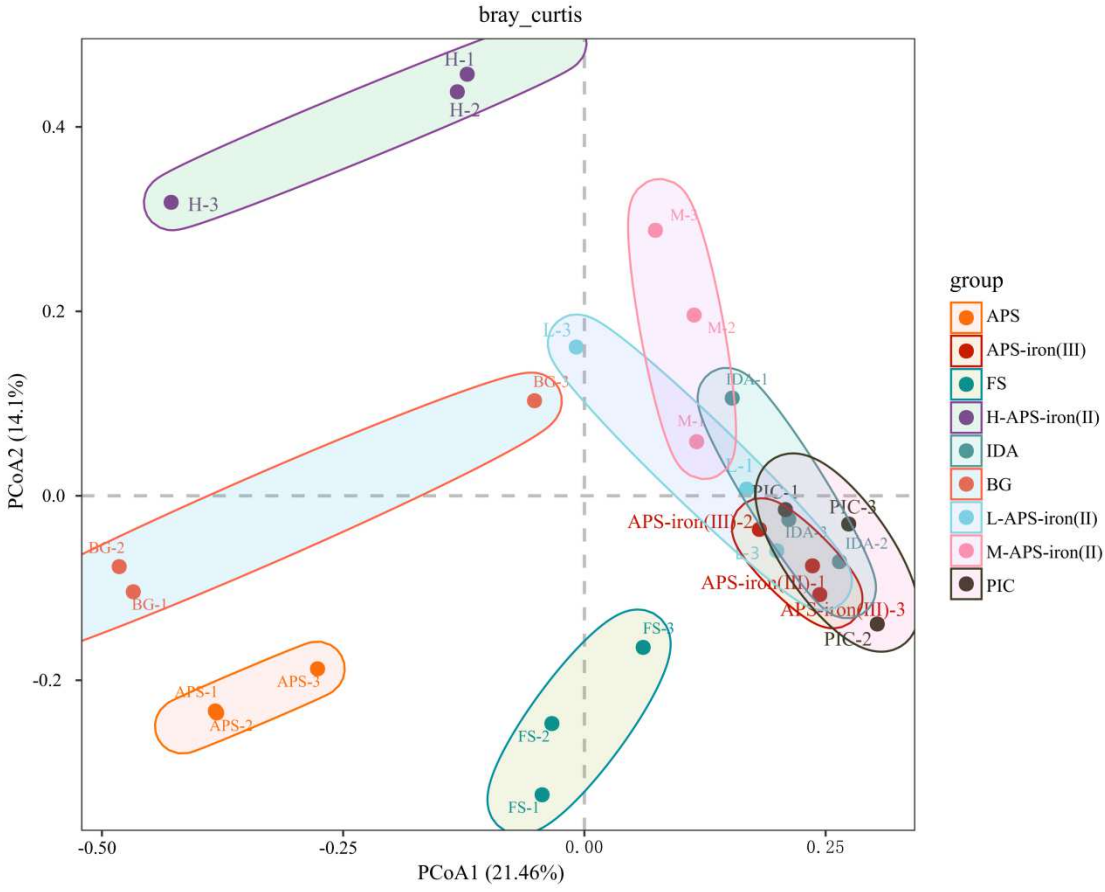


Fig 14 Principal Coordinate Analysis (PCoA) plot

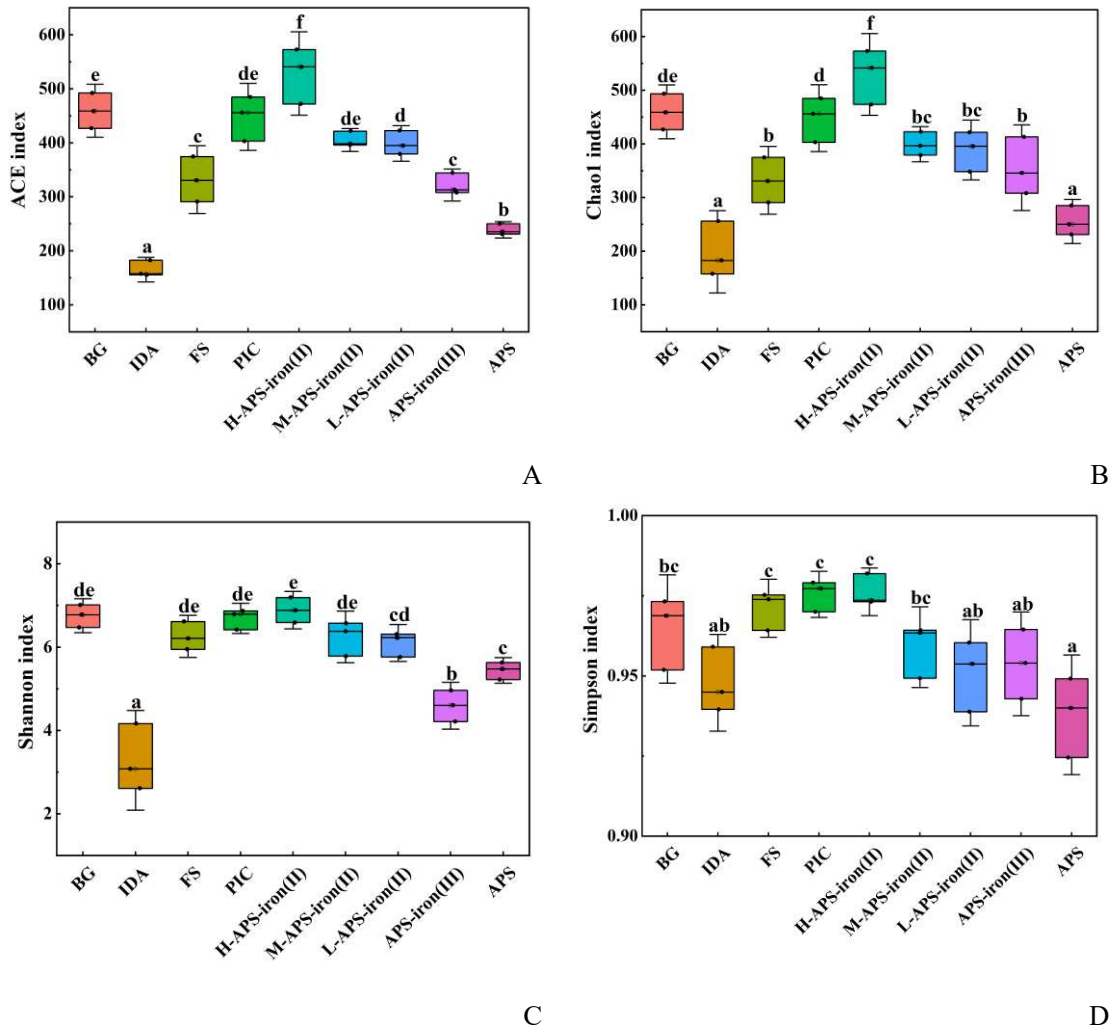


Fig 15 A-ACE index; B-Chao1 index; C-Shannon index; D-Simpson index

Effects of the APS-Iron(II) Complex on Gut Microbial Composition

As shown in Figure 16, the gut microbiota of the normal control group was predominantly composed of Firmicutes, Bacteroidota, and Actinobacteriota at the phylum level, collectively accounting for more than 95% of the total bacterial population.

As illustrated in Figure 17, the IDA model group exhibited a marked reduction in the relative abundance of Firmicutes and Actinobacteriota, accompanied by significant increases in Bacteroidota, Desulfobacterota, and Proteobacteria, indicating substantial disruption of gut microbial homeostasis induced by iron-deficiency anemia.

Compared with the model group, treatment with medium- and high-dose APS-iron(II) significantly increased the relative abundance of Firmicutes while decreasing the abundance of Bacteroidota, thereby partially reversing the gut microbial dysbiosis associated with IDA. These findings suggest that APS-iron(II) supplementation effectively modulates gut microbial composition and contributes to the restoration of microbial homeostasis.

Notably, the APS group exhibited a significantly higher abundance of Actinobacteriota than both the IDA model group and the other treatment groups ($p < 0.05$). This observation suggests that IDA-induced alterations in the intestinal environment may suppress the growth of Actinobacteriota, whereas APS administration may selectively promote the proliferation of this

beneficial bacterial phylum. Consequently, the beneficial effects of APS on intestinal health in IDA rats may be partially mediated through the enrichment of Actinobacteriota and the subsequent improvement of gut microbial ecology.

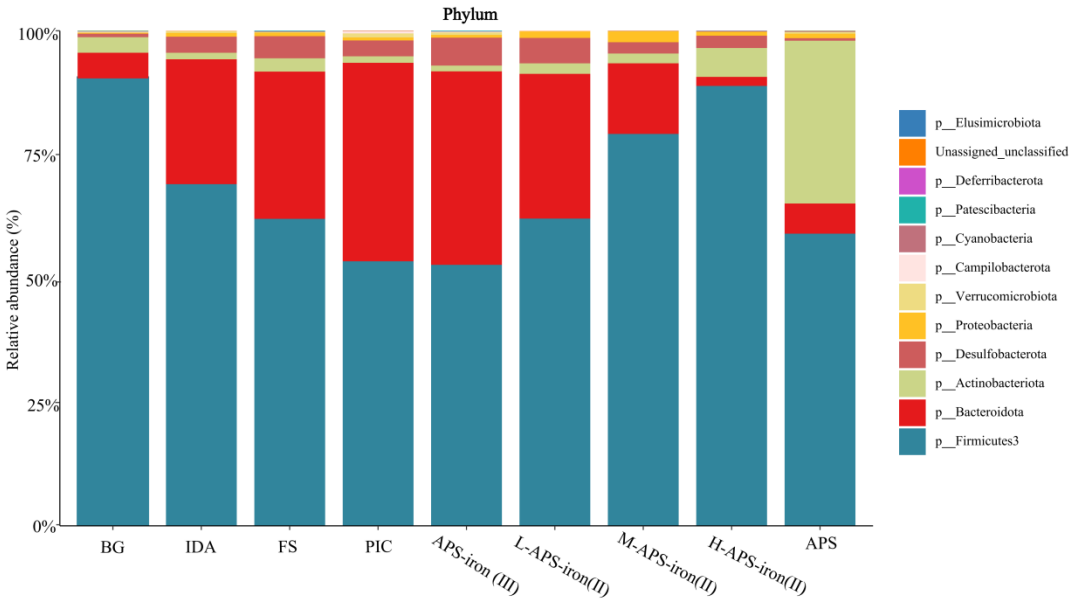


Fig 16 Proportion of microbial communities in the oral cavity

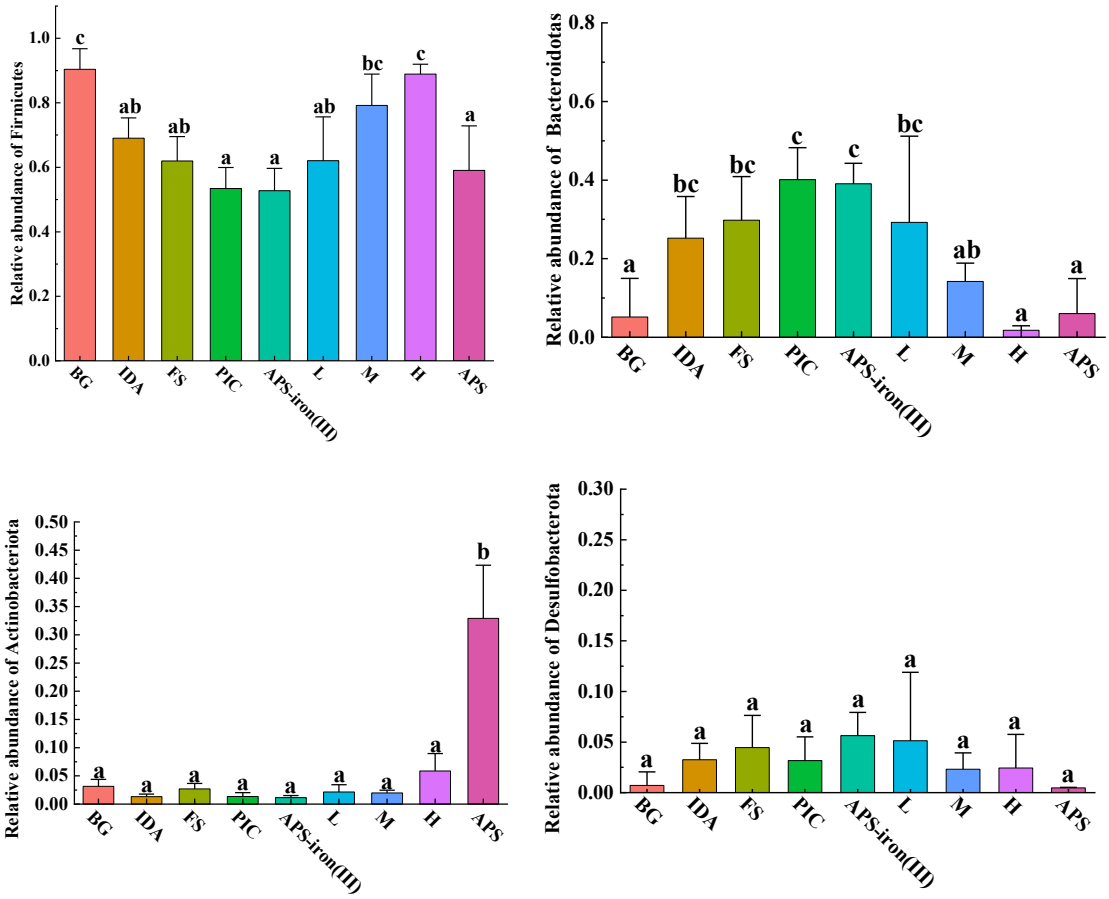


图 17 Firmicutes、Bacteroidota、Actinobacteriota、DesulfobacterotaAbundance difference

Effects of the APS-Iron(II) Complex on Gut Microbiota at the Genus Level

Figure 18 illustrates the relative composition of the gut microbiota at the genus level, while Figure 19 presents the abundance changes of the top 50 genera among the different experimental groups. Compared with the normal control group, the IDA group exhibited a marked reduction in the abundance of beneficial bacteria, including *Enterorhabdus*, *Lactobacillus*, and *Bacillus*. In contrast, several potentially pathogenic genera, including *Staphylococcus*, *Aerococcus*, *Erysipelatoclostridium*, *Candidamus Stoqucfichus*, *Rikenellaceae RC9 gut group*, *Clostridium sensu stricto 1*, *Desulfovibrio*, and *Escherichia-Shigella*, were substantially enriched. The abnormal proliferation of these opportunistic pathogens may contribute to intestinal inflammation, microbial dysbiosis, and impaired gut homeostasis in IDA rats[29-31].

Following APS-iron(II) treatment, the relative abundances of harmful bacteria, including *Staphylococcus*, *Aerococcus*, and *Desulfovibrio*, were markedly reduced. Simultaneously, the abundances of several beneficial genera, including *Turicibacter*, *Romboutsia*, *Enterococcus*, *Weissella*, *Blautia*, *Eubacterium coprostanoligenes group*, *Christensenellaceae R-7 group*, *Bacteroides*, *Parabacteroides*, *Lactobacillus*, and *Bacillus*, were significantly increased[32,33]. Notably, the enrichment of *Romboutsia*, *Enterococcus*, *Lactobacillus*, and *Bacillus* in the APS-iron(II) group was substantially greater than that observed in the ferrous succinate, PIC, and APS-iron(III) groups. These probiotic bacteria are known to contribute to the maintenance of gut microbial homeostasis, enhancement of intestinal barrier integrity, and modulation of host immune responses.

Interestingly, the APS-only group also demonstrated increased abundances of beneficial genera such as *Romboutsia*, *Enterococcus*, and *Blautia*, distinguishing it from the ferrous succinate and PIC groups. This finding suggests that Astragalus polysaccharides themselves possess prebiotic properties capable of selectively promoting beneficial microbial populations.

Collectively, these results indicate that supplementation with the APS-iron(II) complex effectively ameliorates gut microbiota dysbiosis induced by iron-deficiency anemia. Previous studies have demonstrated that beneficial genera such as *Blautia* and *Colidextribacter* can produce short-chain fatty acids (SCFAs), particularly butyrate, which play important roles in alleviating intestinal inflammation and promoting intestinal barrier repair[34,35]. In the present study, *Colidextribacter* was significantly enriched in the APS-iron(III) group, whereas *Blautia* abundance was markedly increased in both the APS group and the medium-dose APS-iron(II) group. These observations suggest that *Blautia* may represent a key microbial taxon involved in the beneficial effects of *Astragalus* polysaccharides on intestinal barrier restoration and gut microbiota remodeling.

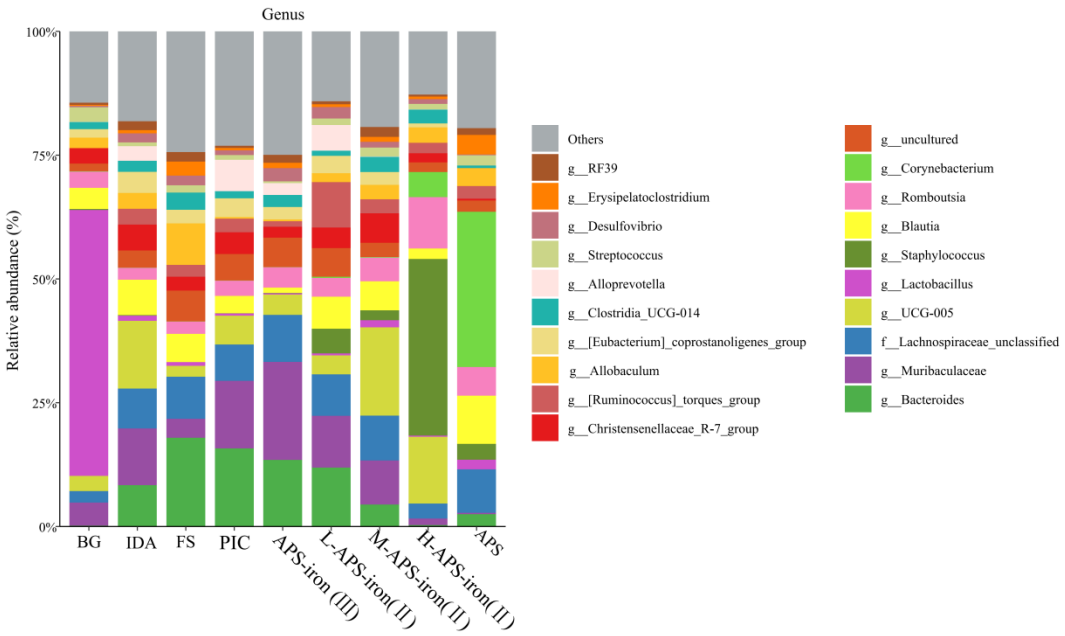


Fig 18 Proportion of bacterial community composition at genus level

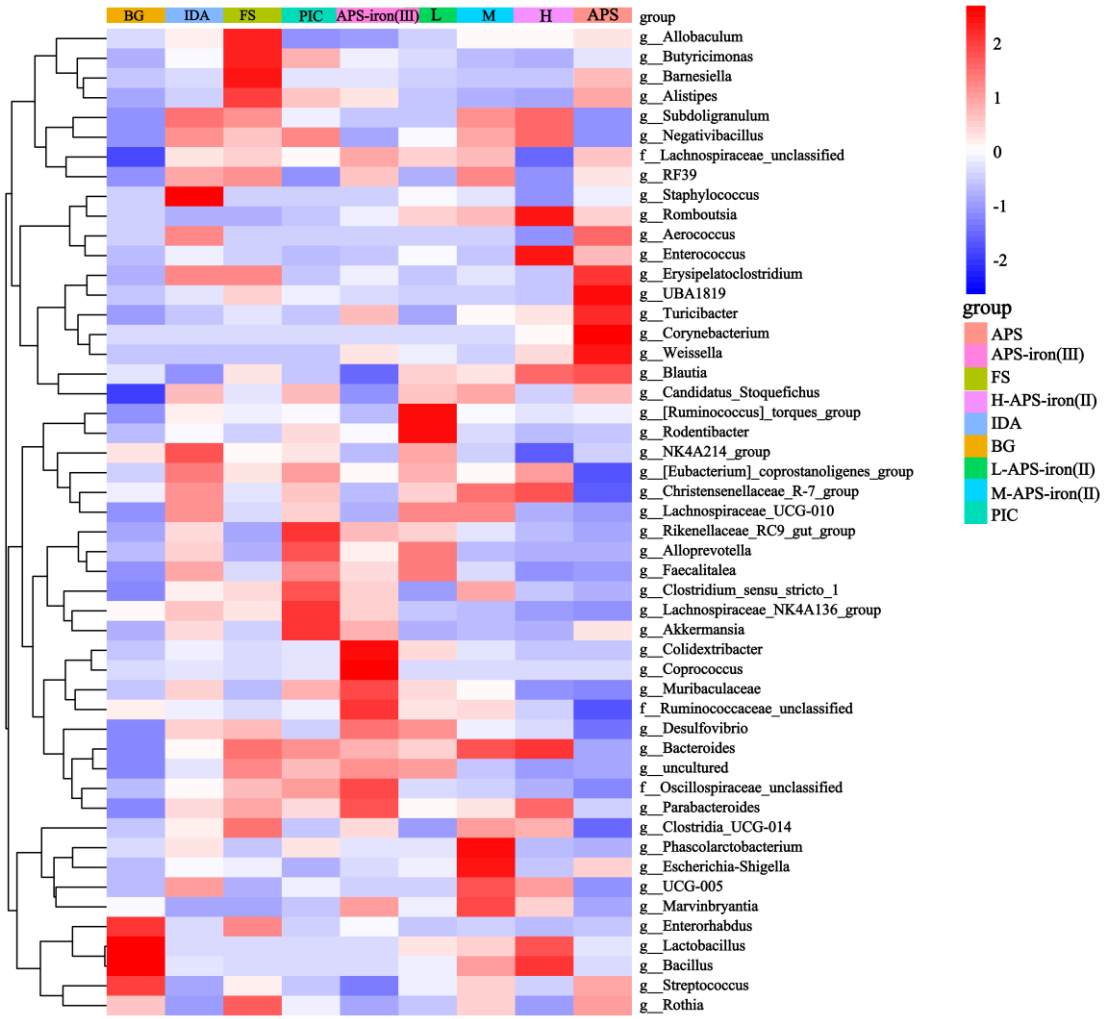


Fig 19 Heat map of genus-level microbial community changes in rat samples

Note: The horizontal axis represents sample names, while the vertical axis denotes the taxonomic annotations of the top 50 species at

the corresponding taxonomic level. The colors in the figure indicate the relative abundance of each species, with a gradient ranging from blue to red representing low to high abundance, respectively.

Correlation Analysis Between IDA-Related Indicators and Gut Microbiota

Spearman correlation analysis was performed to investigate the associations between IDA-related hematological parameters and specific gut microbial taxa, as shown in Figure 20.Following APS–iron(II) treatment, beneficial bacterial genera, including *Turicibacter*, *Romboutsia*, *Blautia*, *Lactobacillus*, *Bifidobacterium*, and *Faecalibacterium*, were positively correlated with erythrocyte-related parameters, while showing negative correlations with total iron-binding capacity (TIBC). These findings suggest that the enrichment of probiotic bacteria is closely associated with improved hematological status and enhanced iron utilization.

In contrast, potentially pathogenic genera such as *Staphylococcus*, *Aerococcus*, *Corynebacterium*, *Holdemanella*, *Streptococcus*, and *Rothia* exhibited negative correlations with erythrocyte parameters and positive correlations with TIBC, indicating their association with impaired iron metabolism and anemia severity. Notably, *Stenotrophomonas* showed a negative correlation with TIBC and a positive correlation with transferrin saturation (TSAT), suggesting a complex role in iron-related metabolic regulation.

Overall, APS-iron(II) treatment effectively restored erythrocyte parameters and improved iron metabolism disturbances induced by IDA, and these effects appear to be closely linked to the modulation of gut microbial composition. The intervention shifted the gut ecosystem from a dysbiotic state characterized by “iron restriction–anemia–microbial imbalance” toward a more balanced state associated with “iron sufficiency–restored erythropoiesis”.

Importantly, this ecological transition is multifaceted. On one hand, it is accompanied by an increase in beneficial metabolic bacteria such as *Turicibacter*, *Romboutsia*, and *Lactobacillus*; on the other hand, improved iron availability also favors the enrichment of iron-dependent opportunistic taxa such as *Stenotrophomonas*[36,37]. The positive correlation between probiotic abundance and improved erythrocyte parameters suggests that these taxa may represent beneficiaries of the restored iron-replete intestinal niche.

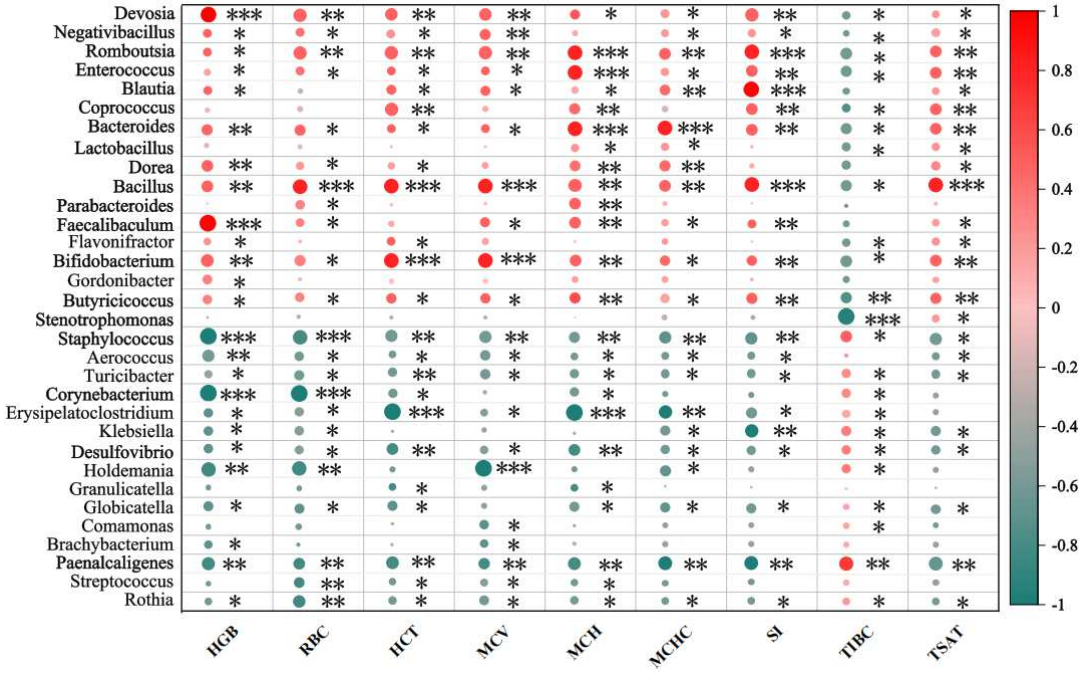


Fig 20 Spearman correlation analysis

Note：*表示 $P \leqslant 0.05$；**表示 $P \leqslant 0.01$；***表示 $P \leqslant 0.001$。

Discussion

In the present study, an APS-iron(II) complex was successfully synthesized through a coordination reaction between Astragalus polysaccharides (APS) and ferrous ions. Chemical composition analysis demonstrated that the iron content of the APS-iron(II) complex was substantially higher than that of the APS-iron(III) complex. Following complex formation, slight reductions in the neutral sugar and protein contents of APS were observed. This phenomenon may be attributed to the coordination of Fe^{2+} with hydroxyl groups on the polysaccharide chains, which enhances the hydrolytic resistance of certain glycosidic residues, while the reaction conditions employed during synthesis may have induced partial protein denaturation and subsequent removal. Monosaccharide composition analysis revealed that glucose remained the predominant monosaccharide constituent of APS-iron(II), indicating that the complexation process did not disrupt the core polysaccharide backbone and therefore preserved the structural basis for its biological activity[38].

Pharmacodynamic evaluation demonstrated that APS-iron(II) administration markedly improved erythrocyte-related parameters in IDA rats. Notably, the medium- and high-dose APS-iron(II) groups exhibited superior therapeutic efficacy compared with the positive control treatments, ferrous succinate and polysaccharide-iron complex capsules, with several hematological indices even exceeding those observed in the normal control group. These findings indicate a pronounced hematopoietic and iron-supplementing effect of APS-iron(II). Analysis of serum iron metabolism parameters further showed that APS-iron(II) significantly increased serum iron (SI) and transferrin saturation (TSAT) while reducing total iron-binding capacity (TIBC), suggesting enhanced iron availability and improved iron utilization[39]. These effects may be attributed to the greater intestinal absorbability of Fe^{2+} and the ability of APS to facilitate the expression of iron transport proteins in the intestinal epithelium[40].

In addition, APS-iron(II) significantly enhanced antioxidant enzyme activities in both serum and liver tissues of IDA rats, indicating an effective capacity to scavenge excessive reactive oxygen

species (ROS) and attenuate oxidative stress. Under iron-deficient conditions, reduced iron availability impairs the synthesis and activity of antioxidant enzymes, thereby exacerbating oxidative damage[41]. APS-iron(II) may counteract this process through a dual mechanism: first, by supplying bioavailable iron required for antioxidant enzyme synthesis; and second, through the intrinsic antioxidant properties of APS, which directly neutralize free radicals. The synergistic interaction between these two components may protect erythrocyte membranes and tissue cells from oxidative injury, thereby promoting erythropoiesis and tissue repair.

Histopathological examination further confirmed the protective effects of APS-iron(II). Treatment markedly alleviated pathological damage in the liver, spleen, and kidneys of IDA rats, restoring tissue morphology toward normal architecture. Moreover, Prussian blue staining demonstrated a substantial increase in hepatic iron storage following APS-iron(II) administration, accompanied by a relatively uniform distribution of iron deposits. These findings suggest that APS-iron(II) effectively replenishes iron stores while minimizing abnormal tissue iron accumulation and reducing the potential risk of iron overload. This beneficial profile may be associated with the controlled-release characteristics of the complex, whereby APS functions as a ligand that gradually releases Fe^{2+}, thereby preventing localized iron overload and iron-induced tissue injury. Furthermore, APS-iron(II) normalized organ indices, particularly those of the heart and spleen, indicating its ability to alleviate compensatory organ hypertrophy induced by chronic iron deficiency and to preserve organ function[42].

It is noteworthy that APS administered alone exhibited limited efficacy in ameliorating IDA. Improvements in hematological parameters, antioxidant capacity, and gut microbial composition were substantially weaker than those observed following APS-iron(II) treatment. These findings suggest that the anti-anemic activity of APS is significantly enhanced following coordination with Fe^{2+}. Mechanistically, APS may improve the stability and bioavailability of ferrous ions, whereas Fe^{2+} provides the essential substrate required for hematopoietic recovery, resulting in a complementary and synergistic therapeutic system. Furthermore, APS-iron(II) consistently outperformed APS-iron(III), likely because Fe^{2+} is more readily absorbed in the intestine and exhibits stronger coordination interactions with APS, thereby facilitating more efficient iron delivery and utilization.

As the “second genome” of the host, the gut microbiota plays a pivotal role in iron metabolism and the pathogenesis of anemia. High-throughput 16S rRNA sequencing revealed that Ace, Chao1, and Shannon diversity indices were significantly reduced in IDA rats, indicating that iron deficiency markedly decreased gut microbial richness and diversity. This alteration is likely associated with iron deficiency-induced changes in the intestinal microenvironment, which suppress the growth of beneficial microorganisms while favoring the proliferation of opportunistic pathogens. At the phylum level, IDA rats exhibited a reduction in the relative abundance of Firmicutes and an increase in Bacteroidota. APS-iron(II) treatment effectively reversed these changes and restored the Firmicutes/Bacteroidota (F/B) ratio toward normal levels. Given the close association of the F/B ratio with nutrient absorption and metabolic homeostasis, these findings suggest that APS-iron(II) may enhance intestinal nutrient utilization and indirectly facilitate iron absorption through modulation of core microbial communities[43].

At the genus level, APS-iron(II) significantly increased the abundance of beneficial bacteria, including *Lactobacillus* and *Bacteroides*, while suppressing potentially detrimental genera such as *Desulfovibrio* and *Clostridium*. Beneficial microorganisms such as *Lactobacillus* and

Bifidobacterium are capable of producing short-chain fatty acids (SCFAs), which lower intestinal pH, enhance iron solubility and absorption, regulate host immune responses, and alleviate intestinal inflammation. In contrast, harmful bacteria such as *Desulfovibrio* may compete with the host for luminal iron, thereby impairing iron acquisition. Consequently, suppression of these microorganisms may contribute to improved iron storage and utilization[44].

Spearman correlation analysis further elucidated the relationship between gut microbiota and IDA-related indicators. Beneficial genera, including *Turicibacter, Romboutsia, Blautia, Lactobacillus, Bifidobacterium*, and *Faecalibacterium*, exhibited significant positive correlations with erythrocyte parameters (HGB, RBC, and HCT) and significant negative correlations with TIBC. In contrast, potentially pathogenic genera such as *Staphylococcus* and *Aerococcus* were negatively correlated with erythrocyte indices. These findings suggest that specific microbial taxa may serve as potential microbial biomarkers of iron-deficiency anemia. By modulating the abundance of these key bacterial genera and restoring microbial homeostasis, APS-iron(II) may improve iron metabolism and erythropoiesis, representing an important mechanism underlying its anti-anemic activity.

Collectively, the present findings demonstrate that APS-iron(II) possesses superior anti-anemic efficacy compared with conventional iron supplements and APS-iron(III). Its therapeutic benefits appear to arise from a multifaceted mechanism involving enhanced iron bioavailability, attenuation of oxidative stress, protection of organ function, restoration of intestinal microbial homeostasis, and promotion of efficient iron metabolism. These results highlight the considerable potential of APS-iron(II) as a novel functional iron supplement and a promising candidate for the prevention and treatment of iron-deficiency anemia.

Conclusion

In the present study, an APS-iron(II) complex was successfully synthesized, and its chemical characteristics and therapeutic efficacy against iron-deficiency anemia (IDA) were systematically investigated. The APS-iron(II) complex contained 75.32 ± 4.28% neutral sugars, 0.94 ± 0.74% protein, and 35.64 ± 3.64% iron. Monosaccharide composition analysis revealed that the complex consisted primarily of glucose (Glc), galactose (Gal), and arabinose (Ara), with a molar ratio of 85.26:10.69:4.05, indicating that the core polysaccharide structure was preserved following complex formation.In vivo experiments demonstrated that APS-iron(II) effectively ameliorated iron-deficiency anemia in rats by promoting body weight recovery, improving erythrocyte-related parameters and iron metabolism indices, attenuating oxidative stress, and alleviating histopathological damage in major organs. Furthermore, 16S rRNA gene sequencing revealed that APS-iron(II) markedly restored IDA-induced gut microbial dysbiosis by enhancing microbial diversity and re-establishing a healthier intestinal microbial community.Collectively, these findings indicate that the APS-iron(II) complex is a promising iron supplement with superior anti-anemic efficacy, attributable not only to its efficient iron supplementation but also to its antioxidant activity and capacity to modulate the gut microbiota. Therefore, APS-iron(II) represents a potential therapeutic candidate for the prevention and treatment of iron-deficiency anemia. Nevertheless, the precise mechanisms governing iron release from the APS-iron(II) complex, as well as its molecular regulation of iron absorption, transport, and systemic iron homeostasis, warrant further investigation.

Authorship Contributions.

W.Y.H. wrote the manuscript. Z.Y. performed data analysis. L.Z.Y. and Z.S.T. conducted sample

preparation. H.Y.L, L.H.F. and H.R.L., designed the research protocol and provided experimental ideas. All authors have read and agreed to the published version of the manuscript.

Ethics Statement.

All animal experiments were conducted in accordance with the Guidelines for Care and Use of Laboratory Animals issued by the National Council for Scientific Research and the requirements of the China Society for Laboratory Animal Science, and were approved by the Ethics and Academic Committee for Laboratory Animals at Shanxi University of Traditional Chinese Medicine (Approval No.: AWE202503028).

Acknowledgements

We would like to extend our sincere gratitude to Jiangsu Sanshu Biotechnology Co., Ltd. for providing the gut microbiota sequencing experiments and data analysis services.

Funding

Survey of Tourism Resources of Authentic Medicinal Materials in Shanxi (2025PY-CXY-002) (Runli He); Traditional Chinese Medicine Science and Technology Innovation Project (2024kjzy009) (Runli He); Shanxi Provincial Administration of Traditional Chinese Medicine Project (2022ZYYC101, 2022ZYYC255) (Runli He); Innovation Capability Cultivation Project of Shanxi University of Chinese Medicine(2022PY-TH-19, 2022PY-TH-20) (Runli He).

Declarations

Competing interests The authors declare no competing interests.

References

1. Kassebaum NJ; GB D 2013 Anemia Collaborators. The Global Burden of Anemia. Hematol Oncol Clin North Am. 2016 Apr;30(2):247-308. https://doi: 10.1016/j.hoc.2015.11.002.
2. Camaschella C. Iron-deficiency anemia. N Engl J Med. 2015 May 7;372(19):1832-43. https://doi: 10.1056/NEJMra1401038.
3. Beard JL. Why iron deficiency is important in infant development. J Nutr. 2008 Dec;138(12):2534-6. https://doi: 10.1093/jn/138.12.2534.
4. Sun B, Tan B, Zhang P, Zhu L, Wei H, Huang T, Li C, Yang W. Iron deficiency anemia: a critical review on iron absorption, supplementation and its influence on gut microbiota. Food Funct. 2024 Feb 5;15(3):1144-1157. https://doi: 10.1039/d3fo04644c.
5. Short MW, Domagalski JE. Iron deficiency anemia: evaluation and management. Am Fam Physician. 2013 Jan 15;87(2):98-104.
6. Tolkien Z, Stecher L, Mander AP, Pereira DI, Powell JJ. Ferrous sulfate supplementation causes significant gastrointestinal side-effects in adults: a systematic review and meta-analy sis. PLoS One. 2015 Feb 20;10(2):e0117383. https://doi: 10.1371/journal.pone.0117383.
7. Cappellini MD, Musallam KM, Taher AT. Iron deficiency anaemia revisited. J Intern Med. 2020 Feb;287(2):153-170. https://doi: 10.1111/joim.13004.
8. Cancelo-Hidalgo MJ, Castelo-Branco C, Palacios S, Haya-Palazuelos J, Ciria-Recasens M, Manasanch J, Pérez-Edo L. Tolerability of different oral iron supplements: a systematic re view. Curr Med Res Opin. 2013 Apr;29(4):291-303. https://doi: 10.1185/03007995.2012.761599.
9. Stoffel NU, Zeder C, Brittenham GM, Moretti D, Zimmermann MB. Iron absorption from supplements is greater with alternate day than with consecutive day dosing in iron-deficient anemic women. Haematologica. 2020 May;105(5):1232-1239. https://doi:

10.3324/haematol.2019.220830.
10. Auerbach M, Deloughery T. Single-dose intravenous iron for iron deficiency: a new paradigm. Hematology Am Soc Hematol Educ Program. 2016 Dec 2;2016(1):57-66. https://doi: 10.1182/asheducation-2016.1.57.
11. Xie J, Wu N, Li D, Xiong S, Dong J, Wang R, Zheng G, Li J. Characterization of Choerospondias axillaris polysaccharide-iron (III) complex and its effect on iron deficiency anemia mice. Int J Biol Macromol. 2025 Mar;296:139759. https://doi: 10.1016/j.ijbiomac.2025.139759.
12. Qi Y, Qiu Z, Li L, Zhao R, Xiang L, Gong X, Zheng Z, Qiao X. Developing garlic polysaccharide-Fe (III) complexes using garlic pomace to provide enhanced iron-supplementing activity in vivo. Food Chem. 2024 Mar 30;437(Pt 1):137819. https://doi: 10.1016/j.foodchem.
13. Xiu W, Wang X, Yu S, Na Z, Li C, Yang M, Ma Y. Structural Characterization, In Vitro Digestion Property, and Biological Activity of Sweet Corn Cob Polysaccharide Iron (III) Complexes. Molecules. 2023 Mar 26;28(7):2961. https://doi: 10.3390/molecules28072961.
14. Lu Q, Xu L, Meng Y, Liu Y, Li J, Zu Y, Zhu M. Preparation and characterization of a novel Astragalus membranaceus polysaccharide-iron (III) complex. Int J Biol Macromol. 2016 Dec;93(Pt A):208-216. https://doi: 10.1016/j.ijbiomac.2016.08.049.
15. Wang P, Wang Z, Zhang Z, Cao H, Kong L, Ma W, Ren W. A review of the botany, phytochemistry, traditional uses, pharmacology, toxicology, and quality control of the Astragalus memeranaceus. Front Pharmacol. 2023 Aug 23;14:1242318. https://doi: 10.3389/fphar.2023.1242318.
16. Lv Y, Xu X, Yang J, Gao Y, Xin J, Chen W, Zhang L, Li J, Wang J, Wei Y, Wei X, He J, Zu X. Identification of chemical components and rat serum metabolites in Danggui Buxue decoction based on UPLC-Q-TOF-MS, the UNIFI platform and molecular networks. RSC Adv. 2023 Nov 7;13(46):32778-32785. https://doi: 10.1039/d3ra04419j.
17. Chen G, Jiang N, Zheng J, Hu H, Yang H, Lin A, Hu B, Liu H. Structural characterization and anti-inflammatory activity of polysaccharides from Astragalus membranaceus. Int J Biol Macromol. 2023 Jun 30;241:124386. https://doi: 10.1016/j.ijbiomac.2023.124386.
18. Wang K, Li L, Xu X, Lu L, Wang J, Wang S, Wang Y, Jin Z, Zhang JZ, Jiang Y. Fe3O4@ Astragalus Polysaccharide Core-Shell Nanoparticles for Iron Deficiency Anemia Therapy and Magnetic Resonance Imaging in Vivo. ACS Appl Mater Interfaces. 2019 Mar 20;11(11):10452-10461. https://doi: 10.1021/acsami.8b18648.
19. Liu P, Wang X, Zhang H, et al. Kinetic studies of internal boiling extraction and other two extraction techniques for polysaccharides from Cortex periplocae[J]. Industrial Crops and Products, 2021, 167: 113554. https://doi.org/10.1016/j.indcrop.2021.113554
20. Bradford MM. A rapid and sensitive method for the quantitation of microgram quantities of protein utilizing the principle of protein-dye binding. Anal Biochem. 1976 May 7;72:248-54. https://doi: 10.1016/0003-2697(76)90527-3.
21. Zheng R, Yang L, Zhang C, Zhang Y, Shi S, Pan Y, Trellu C, Zeng H, Zhou M, Zhang Y. Chelator Denticity Controls Iron Recoveries in the 1,10-Phenanthroline Method via an Enveloping Effect. Environ Sci Technol. 2026 Apr 7;60(13):10332-10343. https://doi: 10.1021/acs.est.5c18732.
22. De Souza LV, Hoffmann A, Fischer C, Petzer V, Asshoff M, Theurl I, Tymoszuk P, Seifert M, Brigo N, Hilbe R, Demetz E, Von Raffay L, Berger S, Barros-Pinkelnig M, Weiss G. Comparative analysis of oral and intravenous iron therapy in rat models of inflammatory anemia and iron deficiency. Haematologica. 2023 Jan 1;108(1):135-149. https://doi:

10.3324/haematol.2022.281149.
23. Jing Y, Zhang S, Li M, Zhang R, Zhang H, Zheng Y, Zhang D, Wu L. Structural characterization and biological activities of polysaccharide iron complex synthesized by plant polysaccharides: A review. Front Nutr. 2022 Sep 30;9:1013067. https://doi: 10.3389/fnut.2022.1013067.
24. Camaschella C, Pagani A, Silvestri L, Nai A. The mutual crosstalk between iron and erythropoiesis. Int J Hematol. 2022 Aug;116(2):182-191. https://doi: 10.1007/s12185-022-03384-y.
25. Xu W, Chen D, Zhang Z, Liu S, Chen C, Sun C, Ni W, Kang X, Shang G, Wang X, Cheng F, Wang Q. Toxicological safety evaluation of Qin-Zhi-Zhu-Dan formula in rats during the treatment and recovery periods. Front Pharmacol. 2022 Aug 25;13:987997. https://doi: 10.3389/fphar.2022.987997.
26. Sonoda A, Nihei M, Shinkawa N, Kakizaki E, Yukawa N. Perls' Prussian blue staining and chemistry of Prussian blue and Turnbull blue. Forensic Sci Int Synerg. 2025 Jul 10;11:100627. https://doi: 10.1016/j.fsisyn.2025.100627.
27. Drury KE, Schaeffer M, Silverberg JI. Association Between Atopic Disease and Anemia in US Children. JAMA Pediatr. 2016 Jan;170(1):29-34. https://doi: 10.1001/jamapediatrics.2015.3065.
28. Wang J, Long Y, Yu G, Wang G, Zhou Z, Li P, Zhang Y, Yang K, Wang S. A Review on Microorganisms in Constructed Wetlands for Typical Pollutant Removal: Species, Function, and Diversity. Front Microbiol. 2022 Apr 5;13:845725. https://doi: 10.3389/fmicb.2022.845725.
29. Dong Z, Liu S, Deng Q, Li G, Tang Y, Wu X, Wan D, Yin Y. Role of iron in host-microbiota interaction and its effects on intestinal mucosal growth and immune plasticity in a piglet model. Sci China Life Sci. 2023 Sep;66(9):2086-2098. https://doi: 10.1007/s11427-022-2409-0.
30. Coffman CN, Varga MG, Alcock J, Carrol-Portillo A, Singh SB, Xue X, Lin HC. Norepinephrine induces growth of Desulfovibrio vulgaris in an iron dependent manner. Anaerobe. 2022 Jun;75:102582. https://doi: 10.1016/j.anaerobe.2022.102582.
31. Malesza IJ, Bartkowiak-Wieczorek J, Winkler-Galicki J, Nowicka A, Dzięciołowska D, Błaszczyk M, Gajniak P, Słowińska K, Niepolski L, Walkowiak J, Mądry E. The Dark Side of Iron: The Relationship between Iron, Inflammation and Gut Microbiota in Selected Diseases Associated with Iron Deficiency Anaemia-A Narrative Review. Nutrients. 2022 Aug 24;14(17):3478. https://doi: 10.3390/nu14173478.
32. John OP, Afolabi KO, Ngene AC, Tanimowo WO, Adewoyin MA, Osho MB, Reuben RC. Enterococcus Species: Multifaceted Probiotic Potential and Safety Considerations. Microorganisms. 2026 Apr 2;14(4):815. https://doi: 10.3390/microorganisms14040815.
33. Junaid M, Lu H, Li Y, Liu Y, Qi ZQ, Liu K, Yan J. Probiotic Therapy with Lactobacillus Restores Gut Microbiota and Modulates Immunity in Salmonella-Infected Mice. Foodborne Pathog Dis. 2026 Mar 11:15353141261430303. https://doi: 10.1177/15353141261430303.
34. Holmberg SM, Feeney RH, Prasoodanan P K V, Puértolas-Balint F, Singh DK, Wongkuna S, Zandbergen L, Hauner H, Brandl B, Nieminen AI, Skurk T, Schroeder BO. The gut commensal Blautia maintains colonic mucus function under low-fiber consumption through secretion of short-chain fatty acids. Nat Commun. 2024 Apr 25;15(1):3502. https://doi: 10.1038/s41467-024-47594-w.
35. Liang L, Liu L, Zhou W, Yang C, Mai G, Li H, Chen Y. Gut microbiota-derived butyrate regulates gut mucus barrier repair by activating the macrophage/WNT/ERK signaling pathway. Clin Sci (Lond). 2022 Feb 25;136(4):291-307. https://doi: 10.1042/CS20210778.

36. Pessoa RBG, de Oliveira WF, Correia MTDS, Fontes A, Coelho LCBB. Aeromonas and Human Health Disorders: Clinical Approaches. Front Microbiol. 2022 May 31;13:868890. https://doi: 10.3389/fmicb.2022.868890.
37. Kümmerli R. Iron acquisition strategies in pseudomonads: mechanisms, ecology, and evolution. Biometals. 2023 Aug;36(4):777-797. https://doi: 10.1007/s10534-022-00480-8.
38. Liu M, Wang Y, Wang R, Zong W, Zhang L, Wang L. Preparation and Performance Evaluation of Polysaccharide-Iron Complex of Eucommia ulmoides. Foods. 2024 Jul 22;13(14):2302. https://doi: 10.3390/foods13142302.
39. Jing Y, Zhang S, Li M, Zhang R, Zhang H, Zheng Y, Zhang D, Wu L. Structural characterization and biological activities of polysaccharide iron complex synthesized by plant polysaccharides: A review. Front Nutr. 2022 Sep 30;9:1013067. https://doi: 10.3389/fnut.2022.1013067.
40. Chen Y, Wang J, Li J, Zhu J, Wang R, Xi Q, Wu H, Shi T, Chen W. Astragalus polysaccharide prevents ferroptosis in a murine model of experimental colitis and human Caco-2 cells via inhibiting NRF2/HO-1 pathway. Eur J Pharmacol. 2021 Nov 15;911:174518. https://doi: 10.1016/j.ejphar.2021.174518.
41. Lin L, Yin X, Guan Y. Decoding iron deficiency in cancer: mechanisms, immune modulation, and therapeutic potential. Front Nutr. 2025 Oct 20;12:1650929. https://doi: 10.3389/fnut.2025.1650929.
42. Yang H, Zang X, Jin X, Chen J, Lv Y, Lv Z. Efficacy of polysaccharide iron complex in IDA rats: A comparative study with iron protein succinylate and ferrous succinate. Biomed Pharmacother. 2024 Jan;170:115991. https://doi: 10.1016/j.biopha.2023.115991.
43. Chen JH, Wang Y, Pan J, Lu LW, Yu J, Liu B, Chen F, Deng H. Prebiotic Oligosaccharides Enhance Iron Absorption Via Modulation of Protein Expression and Gut Microbiota in a Dose-Response Manner in Iron-Deficient Growing Rats. Mol Nutr Food Res. 2022 May;66(10):e2101064. https://doi: 10.1002/mnfr.202101064.
44. Mayneris-Perxachs J, Moreno-Navarrete JM, Fernández-Real JM. The role of iron in host-microbiota crosstalk and its effects on systemic glucose metabolism. Nat Rev Endocrinol. 2022 Nov;18(11):683-698. https://doi: 10.1038/s41574-022-00721-3.